Early Elevated IFNα Identified as the Key Mediator of HIV Pathogenesis and its low level a Hallmark of Elite Controllers

Robert Gallo (rgallo@ihv.umaryland.edu)
Univ. Maryland, School of Medicine

Hélène Buanec
Université de Paris

Valérie Schiavon
Université de Paris

Marine Mérandet
INSERM

Alexandre Howkit
Laboratory for Genomics Foundation Jean Dausset-CEPH

David Bergerat
Université de Paris

Fombellida Lopez C
University of Liege

Armand Bensussan
INSERM-UMR 976 https://orcid.org/0000-0002-0409-2497

Jean-David Bouaziz
Université de Paris

Arsène Burny
Université of Liège

Gilles Darcis
University of Liege, Switzerland

HONGSHUO SONG
University of Maryland School of Medicine, Baltimore

Mohammad Sajadi
Institute of Human Virology, University of Maryland School of Medicine

Shyamasundaran Kottilil
Institute of Human Virology at the University of Maryland School of Medicine

Daniel Zagury
21CBIO

Article

Keywords:

Posted Date: May 11th, 2023

DOI: https://doi.org/10.21203/rs.3.rs-2813601/v1

Additional Declarations: There is **NO** Competing Interest.

Early Elevated IFNα Identified as the Key Mediator of HIV Pathogenesis and its low level a Hallmark of Elite Controllers

Authors: Hélène Le Buanec[1], Valérie Schiavon[1], Marine Merandet[1], Alexandre How-Kit[2], David Bergerat[1], Céline Fombellida-Lopez[3], Armand Bensussan[1], Jean-David Bouaziz[1,4], Arsène Burny[5,6], Gilles Darcis[3], Hongshuo Song[7], Mohammad M. Sajadi[6,7], Shyamasundaran Kottilil[6,7,8], Robert C. Gallo[6,7*], and Daniel Zagury[9].

Affiliations:

[1]Université de Paris; INSERM U976, HIPI Unit, Institut de Recherche Saint-Louis, F-75010 Paris, France.

[2]Laboratory for Genomics Foundation Jean Dausset-CEPH; Paris France

[3]Laboratory of Infectious Diseases, GIGA-I3, GIGA-Institute University of Liege; 4000 Liege, Belgium

[4]Dermatology Department, Hôpital Saint-Louis, Assistance Publique-Hôpitaux de Paris (AP-HP), Paris, France

[5]Laboratory of Molecular Biology, Gembloux Agrobiotech,University of Liège ;Belgium

[6]Global Virus Network, Baltimore, MD 21201, USA.

[7]Institute of Human Virology, School of Medicine, University of Maryland; Baltimore MD, 21201, USA, Department of Medicine, School of Medicine, University of Maryland, Baltimore, MD, 21201, USA.

[8]University of Maryland School of Medicine; Baltimore, MD 21201, USA, Program in Oncology, Marlene and Stewart Greenebaum Comprehensive Cancer Center, University of Maryland, Baltimore, MD 21201, USA.

[9]21CBIO; Paris France.

Co last authors: Gallo RC. And Zagury D.

*Corresponding author. Email: rgallo@ihv.umaryland.edu

Abbreviations:

ADO: Adenosine

ATP: adenosine triphosphate

AMP: Adenosine monophosphate

cART: combined antiretroviral therapy

$CD8^+$supp: cytotoxic $CD8^+$ suppressive T-cell

CM: Central Memory

CTL: $CD8^+$ cytotoxic T lymphocyte

DC : Dendritic cells

EC: Elite Controller

EM: Effector Memory

HD: Healthy Donor

IR: Immune Reaction

mRNA : messenger ribonucleic acid

NK : Natural Killer

TEMRA : Terminal Differentiated Effector Memory

Abstract

Advances in HIV therapy came from understanding its replication. Further progress toward "functional cure" -no therapy needed as found in Elite Controllers (EC)- may come from insights in pathogenesis and avoidance by EC. Here we show that all immune cells from HIV-infected persons are impaired in non-EC, but not in EC. Since HIV infects few cell types, these results suggest an additional mediator of pathogenesis. We identify that mediator as elevated pathogenic IFNα, controlled by EC likely by their preserved potent NK-cells and later by other killer cells. Since the earliest days of infection predict outcome genetic or chance events must be key to EC, and since we found no unique immune parameter at the onset, we suggest a chance infection with a lower HIV inoculum. These results offer an additional approach toward functional cure: a judicious targeting of IFNα for all non-EC patients.

Introduction

Potent anti-retroviral therapy (ART) was chiefly developed through advances in understanding stages and molecular events involved in HIV replication. However, these advances have not led to a "functional cure" in which no further therapy is needed to suppress virus resurgence and immune decline. One approach is development of longer lasting drugs and better delivery. An additional approach is to attempt a greater understanding of HIV pathogenesis. A small group of HIV-infected patients, with undetectable viral load without therapy, known as elite controllers (EC) (< 0.5%), were found by several clinical investigators and championed by Steven Deeks and Bruce Walker (*1*) who suggested that perhaps the EC status could be mimicked to reach a "functional cure*"(2).* Individuals with a genotype including HLA_{B57+} (EC_{B57+}), which share the Bw4 serotype with the KIR3DL1 allele were found more prone to become EC *(3)*. However, not all EC are HLA_{B57+} *(4)*. Consequently, other mechanisms must contribute to the EC status.

Given our long-term studies on the pathogenic (high levels) effects of IFNα in AIDS *(5,6),* we questioned whether control of the pathogenic effects of IFNα could be a major immune mechanism that is controlled by EC. Indeed, as described in the extended data Table 1, our initial and other reported studies showed that elevated IFNα exerts several pathogenic effects. These occur first at the innate phase of an IR by inhibiting IL-7-induced T-cell proliferation controlling T-cell homeostasis *(7);* second, at the initiation phase of the adaptive IR by inhibiting proliferation of $CD4^+$ T helper cells *(8)* ; third, by differentiating T-cells to suppressive IL-10-Tr1 cells *(9,10)*. Systemic IFNα (type I IFN) and mucosal IFN-lambda (IFNλ) (type III IFN) both exert antiviral activities via IFN-stimulated genes (ISGs) *(11),* albeit with different kinetics of ISGs induction and distinct cell targets expressing specific receptors. IFNAR1 and IFNAR2 are constitutively expressed on virtually all nucleated cells such as $CD4^+$T-cells, whereas at homeostasis IFNλ receptors are constitutively expressed on epithelial cells and only in a selected pool of immune cells *(12).* Consequently, the $CD4^+$T-cells are functionally hampered by elevated IFNα at the initiation of the IR adaptive phase, but not by IFNλ even at high levels (extended data Fig. 1). interestingly, a 2023 report shows the efficacy of therapeutic administration of IFNλ in early covid patients *(13)*.

The conclusion that elevated IFNα is a central mediator of HIV pathogenesis is supported by the literature and by results throughout this paper. First, genetic studies have identified polymorphisms in IFN type 1 and type 3 pathways as contributing to variable responses to HIV infection *(14).* Second, SIV-infected African green monkeys do not express elevated levels of IFNα and avoid development of AIDS *(15).* By contrast SIV-infected rhesus macaques develop AIDS and have high level of serum IFNα *(16).* Third, clinical trials results from the EURIS phase 2B placebo control, carried out in 5 hospital centers from 1996-1998 on 240 patients, who had not received combined ART, were based on the induction of anti-IFNα antibodies by an active vaccine approach to lower IFNα. Vaccine responders achieved all study endpoints,

including a lower occurrence of HIV-related events, improved $CD4^+$T-cell counts and reduced viral load correlating with the rise of anti-IFNα Abs *(17).* Fourth, we show that IFNα induces a series of immune cell abnormalities in untreated non-EC patients (extended data Table 1 and extended data Fig. 1).

We found that HIV untreated patients (non-EC) have abnormally high concentrations of serum IFNα and a high frequency of phenotypic alterations in all immune cell types. These alterations are known effects of IFNα (extended Fig. 1-2 and extended Table 1). In contrast EC show minimal abnormal immune cell alterations. We further identified potential immune mechanisms enabling each EC to control viral replication by its own immune capacity. Finally, we hypothesized that EC control of IFNα is at least partially circumstantial, namely a fortuitous infection with a low dose of HIV. Since IFNα levels at the primary phase of the acute infection correlate with virus titer, we surmise a vicious circle of HIV → IFNα → more HIV → elevated IFNα → more HIV etc may be the critical factor contributing to loss of virus replication control by non-EC, and in the accompanying manuscript we described the mechanism leading to this vicious circle.

Results

As detailed in methods, the study compares in untreated non-EC, EC and HD 1) IFNα and IFNλ2 serum concentration, 2) the distribution of immune cell subsets, and 3) the frequency of cell markers associated with immune dysfunction. These include abnormal expression of checkpoint receptors or molecules controlling immune cells function such as 1) inhibitory checkpoint receptors (PD1, CTLA-4) leading cells to an exhaustion stage *(18)*; 2) cell receptor markers of activation/differentiation (CD25/CD38/HLA-DR) associated with chronic immune activation *(19)*; 3) checkpoint receptors controlling pericellular levels of immunosuppressive adenosine (CD39 ectonucleotidases; CD26 harboring adenosine deaminase) *(20)*; 4) apoptotic

cell receptors (CD95) and 5) soluble suppressive mediators (IL-10). This phenotypic study focuses particularly on cytotoxic NK-cells, HLA1a-(B)-restricted $CD8^+$CTL and HLA1b-(E)-restricted $CD8^+$ suppressive cells ($CD8^+$supp). Interestingly, $CD8^+$supp, which lyse abnormal $CD4^+$T-cells expressing HIV-peptides in a HLA-E-restricted presentation, are also present in other chronic inflammatory diseases including autoimmune diseases *(21)*, cancer *(22)* and other microbial infections *(23).*

IFNα is elevated in HIV-infected non-EC and modifies the distribution of blood immune cell types.

Blood immune cell types distribution, from non-EC compared to EC and HD, analyzed by Principal Component Analysis (PCA) shows that non-EC and HD cluster separately, while EC overlap both (Fig. 1A). Fig. 1B and 1C document the distinct proportion of circulating immune cell types in non-EC, EC and HD. We found that IFNα, but not IFNλ2, serum concentration was abnormally increased in non-EC compared to HD and the large majority of EC (Fig. 1D). We also found a positive correlation between between IFNλ2 and IFNα serum levels in EC but not in non-EC patients (Fig. 1E1). Moreover, serum IFNλ2 concentration was negatively associated with $CD4^+$T-cells, and positively with $CD8^+$T-cells frequency in non-EC (Fig. 1E2-3).

Elevated IFNα induces an abnormal frequency and phenotypic alterations of NK-cells and other innate cell types in non-EC but not in EC.

NK-cells are a heterogeneous population of immune cells *(24),* as shown by spade analysis (Fig. 2A1) and dot plots (Fig. 2A2). As previously reported *(25),* non-EC had less early and mature NK-cells than HD (2.58% vs 4.61% and 48.1% vs 83.2%), and much more terminal NK-cells (17.91% vs 2.84%) (Fig. 2A3). EC and HD displayed similar proportions of NK-cell subsets.

In the mature NK subset, activating markers Helios, NCR and GrzB/perf, were less frequent in non-EC than in EC and HD (Fig. 2B1-2). In contrast, inhibitory Killer-cell immunoglobulin-like receptors (iKIRs), which bind HIV-peptides presented on HLA-1b in activated $CD4^+$T-cells as well as inhibitory checkpoint receptors PD1 or CD39, leading cells to an exhaustion-like status *(18),* were overexpressed in non-EC compared with EC and HD (Fig. 2B3-4). Noteworthy, CD38 and HLA-DR were prevalent in non-EC mature NK-cells. In addition, there was positive correlations between IFNα levels and the frequency of $iKIR^+$ mature NK-cells, terminal NK-cells and $iKIR^+$ terminal NK-cells (Fig. 2C). This is consistent with IFNα enhancing the development of non-functional NK-cells. Further, indicative of this loss of function among NK-cells in non-EC was the presence of the activation marker NKG2D, only weakly expressed on early NK-cells (Fig. 2D1) and the apoptotic marker CD95 highly expressed on mature NK-cells (Fig.2D2) thereby reducing their cytotoxic activity and increasing their propensity to apoptosis respectively.

To investigate whether elevated IFNα induced these altered NK-cell subset distribution and surface phenotypes, we treated *in vitro* purified NK-cells with increasing dose of IFNα. We found that elevated IFNα inhibited NK-cells viability and proliferation capability in a dose-dependent manner (Fig. 2E1-2). Furthermore elevated IFNα reduced CD56 expression in $CD56^{dim/neg}$NK-cells (Fig. 2E3), leading to a decrease of mature NK-cells frequency and a concomitant increase of terminal NK-cells percentage (Fig. 2E4). Addition of increasing amounts of IFNα in NK-cell culture induced a dose-dependent decrease of NKG2D expression in early (Fig. 2E5) and increase of CD95 expression in mature NK-cells (Fig. 2E6). In summary the NK-cell abnormalities observed in non-EC can be in large part induced by elevated IFNα levels.

As to other innate immune cells, $CD11c^{-}/CD123^{+}$ pDC frequency is lower in non-EC than in EC (13.4% versus 32.5 % respectively) (extended data Fig. 4A). This observation was previously made by others *(26).* γδ T-cells show an abnormally high expression of inhibitory checkpoint receptors in non-EC (extended data Fig. 4B). The expression of these checkpoint receptors is triggered directly by IFNα including CD38 *(27),* HLA-DR *(27)* and indirectly by loss of CD26 *(28).*

Elevated IFNα alters immune cell homeostasis in non-EC compared to HD and a majority of EC.

Homeostatic disturbances of T-cell subsets after HIV infection are hallmarks of early disease. We investigated the maintenance of $CCR7^{+}CD4^{+}$ and $CD8^{+}$T-cells in the 3 groups. As anticipated, a lower frequency of both T-cell subsets was observed in non-EC compared to EC and HD (extended data Fig. 4C1-2). In addition, negative correlations were observed between $CD4^{+}$ and $CD8^{+}$CM T-cell frequency and serum IFNα levels in HIV-patients (extended data Fig. 4C3-4) reflecting the pathogenic inhibitory effects of IFNα on IL-7-induced homeostatic T-cell proliferation *(7)* occurring in $CD4^{+}$ and $CD8^{+}CCR7^{+}$T-cells homing to lymph nodes *(29)*. Interestingly, whereas the frequency of EC_{B57+} $CD8^{+}$CM is similar to HD, the frequency of EC_{B57-} $CD8^{+}$CM is reduced, albeit at a lesser degree than in non-EC (extended data Fig.4C5 and Table 1). The maintenance of T-cell homeostasis observed in EC_{B57+} but not EC_{B57-} (Table 1) may be accounted for by the homology between HLA_{B57+} and NK iKIR (specifically 3DL1 allele) sharing the bw4 serotype. Therefore, $iKIR^{+}$ NK do not recognize HLA_{B57} peptide epitopes, and NK-cells killing is not inhibited. This enables the unaltered EC_{B57+} $iKIR^{+}$ NK cells lysis of infected $CD4^{+}$T-cells resulting in reduction of the viral load and its correlated IFNα production level *(30).* Consequently, upon TCR stimulation, we observed a reduced

percentage of CM T-cells which differentiate into $CD4^+$T helper and cytotoxic $CD8^+$T-cells in non-EC but not in EC_{B57+}.

Besides direct killing of some $CD4^+$T-cells by HIV, during the acute phase of infection, early HIV regulatory proteins Nef and Tat are released. Nef reduces cellular HLA-1a expression ([31]), and Tat enhances IFNα production by macrophages *(5),* thus contributing along with high HIV to the elevated IFNα. This in turn leads to NK-cells phenotypic and functionnal alterations. The outcome is a lack of early lysis of infected $CD4^+$T-cells in most HIV-infected patients, as shown here. These immune cell alterations are spared in EC.

Elevated IFNα in non-EC is associated with a high frequency of IFNα-induced phenotypic abnormalities of $CD4^+$ and $CD8^+$T-cells.

We first identified the major circulating $CD4^+$Tconv (T helper $Foxp3^-$) cell subsets at different maturation stages based on their surface expression of CCR7 and CD45RA *(32)*. SPADE analysis done on Tconv (Fig. 3A1) and histograms (Fig. 3A2) show that the frequency of their subtypes vary in both non-EC and EC compared to healthy donors. Both EC and non-EC have significantly lower frequencies of naive $CD4^+$T-cells compared with HD. While EC have higher CM and TEMRA, non-EC have higher EM and TEMRA. (Fig. 3A2). We then explored changes in activation/exhaustion phenotypes in $CD4^+$T-cell subsets in non-EC compared to EC and HD. The absence (CD26, CD25, CD28) or increase (CD38, HLA-DR,CD39, PD1 and CTLA-4) of these markers are linked to an exhaustion-like state associated with lack of function *(18)*. Each Tconv subset display an altered distinct phenotypic profile in non-EC compared to EC and HD (Fig. 3A3 and extended data Fig.5). CM, EM and TEMRA from non-EC exhibited significantly higher phenotypic alteration scores (see methods) compared to those from EC (Fig. 3A4). These phenotypic abnormalities correspond in large part to the IFNα effects on $CD4^+$T-cells in culture

(extended data Table 1 and extended data Fig.1). This is consistent with one key HIV pathogenic mediator, namely the effect of elevated IFNα in non-EC. Furthermore, positive correlations are observed between the expression levels of different abnormally expressed markers studied in the $CD4^+$CM in non-EC but not in EC (extended data Fig.5e). We then investigated the circulating $CXCR5^+CD45RO^+CD4^+$ TFH (cTFH) that govern the B-cells hypersomatic mutation and Ig isotype commutation in follicular lymph nodes. Compared with HD, non-EC had lower frequency of cTfh-cells (Fig.3A5a), and, on these cells, they exhibited lower CXCR5 expression level (Fig. 3A5b) and higher coexpression of CD38 and HLA-DR (Fig. 3A5c). In addition, while similar frequency of $CD19^+$B-cells was observed between the two studied groups (Fig. 3A6a), non-EC had a reduced percentage of $CXCR5^+$B-cells (Fig. 3A6b) and on these cells CXCR5 expression level was lower (Fig. 3A6c). As to the regulatory $CD4^+$T-cell subset ($CD4^+Foxp3^+$), their frequency and function were altered in non-EC but not in EC (Fig. 3B). Their proportion was increased (Fig. 3B1-2) and the percentage of non-functional $CD25^-$ Treg variant *(28)* was enhanced (Fig. 3B3-4). Once again, the serum IFNα level significantly correlated with this alteration (Fig. 3B5). In addition, memory $CD4^+$Treg phenotypic abnormalities associated with IFNα were multiple in non-EC but minimal in EC. (Fig. 3B6).

We next performed similar analysis on $CD8^+$T-cells in non-EC compared to EC and HD. We examined four well-defined $CD8^+$T-cell subsets as above for the Tconv. Distinct distributions of $CD8^+$T-cell subsets in the three groups were found, as shown by viSNE analysis (Fig. 4A1) and histograms (Fig. 4A2). Both EC and non-EC had a significantly lower frequency of naive $CD4^+$T-cells compared with HD. Non-EC also had lower CM and higher EM and TEMRA than HD and EC (Fig. 4A1-2). As for the Tconv subsets, each $CD8^+$T-cell subset had a distinct pattern of phenotypic alterations in non-EC compared to EC and HD. Non-EC CM and TEMRA had a higher phenotypic alteration score than those of EC (Fig. 4A3-5). A large majority of

these inhibitory checkpoints receptors are induced by IFNα (extended data Table 1). Furthermore, as described in Fig. 4A6, in non-EC, positive correlations were observed between the expression levels of the various studied markers in $CD8^+$CM. $CD8^+$ HIV-specific cytotoxic T-cells are comprised of effector HLA-1a-restricted CTL and HLA-E-restricted $CD8^+$supp carrying iKIRs, the human analog of Ly49, which characterize murine $CD8^+$supp *(33,*34). HLA-1a-(B) and HLA-1b-(E)-presenting HIV-peptide tetramers recognizing CTL (Fig. 4B1) and $CD8^+$supp (Fig. 4B2) respectively. This allowed us to distinguish and phenotypically characterize the two types of cytotoxic $CD8^+$T-cells: CTL ($CD8^+$, TEMRA, GrzB/$perf^+$, $iKIR^-$, $Helios^-$) and $CD8^+$supp ($CD8^+$, TEMRA, GrzB/$perf^+$, $iKIR^+$, $Helios^+$). We found similar CTL frequency in EC and non-EC (81.05 % vs 74.15 %) (Fig. 4B3), but the inhibitory checkpoint receptors level was significantly higher in non-EC than in EC and HD (Fig. 4B5), again fitting with the effect of elevated IFNα. This leads to greater CTL activity of EC. As to the $CD8^+$supp, non-EC had a slightly higher percentage of $CD8^+$supp than EC (25.85% vs 18.95%) (Fig. 4B4) with a more pronounced exhaustion-like stage (CD38, CD39, HLA-DR) or downregulated markers (CD26) (Fig. 4B6), all of which can be induced by IFNα. Of note, similar to the CTL, the $CD8^+$supp frequency of EC is also variable from one donor to another.

The minimal anti-HIV immune cells phenotypic defects and the control of HIV replication in EC is linked to control of IFNα.

PCA analysis (Fig. 5A1) and heatmaps (Fig. 5A2) show that EC, whether expressing HLA_{B57} (EC_{B57+}) allele or not (EC_{B57-}), have a distinct blood immune cell profile variable in each individual. They express a few phenotypic alterations in large part induced by elevated IFNα (Compare to non-EC, Fig. 1D).

To further identify which anti-HIV immune function, uncommonly found in humans, could account for the control of HIV replication in each EC, we investigated which anti-HIV factor(s) known to neutralize circulating virions or to lyse infected $CD4^+$T-cells might contribute to the maintenance of the EC status .

Considering the frequency of elevated IFNα -induced immune cell types phenotypic anomalies in non-EC, we examined serum IFNα levels in all patients. The median in non-EC is 95 fg/mL and in EC 18 fg/mL. In our American HIV patient's cohort, 16 out of 20 non-EC compared to 3 out of 18 EC, showed a higher IFNα level (Table 1). Interestingly, among the 3 EC expressing elevated serum IFNα, EC11 and EC52 compensate their high IFNα, level by the expression of NK-cells activating NKG2C receptor contributing to early lysis of infected $CD4^+$T-cells. EC68 cell sample was not available (Table 1). Regarding IFNλ, it is notable that only EC51 had high level compared to other EC (32000 fg/mL vs 1027 fg/mL). pDC frequency were higher in EC compared to other HIV-infected persons (32% versus 14%, Table 1). It is unlikely that greater numbers of pDC be a key immune parameter causing the EC state and in control of elevated IFNα. Rather it is likely that their increase is a consequence of the better control of IFNα in the early days of infection, thereby avoiding its negative impact.

Given that NK-cells act at the onset of infection, and before the virus setpoint, we focused on them in both EC_{B57+} and EC_{B57-} . Mature EC_{B57+} NK-cells (9 out of 10 tested) are predominantly $iKIR^-$, whereas most mature EC_{B57-} NK-cells are $iKIR^+$ (Fig. 5A2 and 5B1). Therefore, these EC_{B57+} NK-cells have the functional capacity to lyse infected $CD4^+$T-cells, releasing circulating virions as early as the beginning of the IR. It is notable that one EC_{B57-} (EC13) behaved as an EC_{B57+}, but its mechanism is as yet not defined (Table 1). Interestingly, in EC_{B57-} mature NK-cells the expression of NKG2C counterbalance the inhibitory iKIR signals (Fig. 5B3) and allow

these NK-cells to kill infected $CD4^+$T-cells expressing HIV-peptides in an HLA-E presentation, thus reducing the viral load in EC_{B57-}.

The percentage of circulating $CD8^+$CM was relatively high in EC_{B57+} (identical to HD median: 10% vs 10%) but reduced in EC_{B57-} albeit higher than in non-EC (median: 6% vs 4%, Table 1) (Fig 5B4 and extended data Fig.4C5). Consequently, the frequency of CTL derived from the differentiation of $CD8^+$CM was lower in EC_{B57-} compared to EC_{B57+} . It results in higher frequency of CTL than $CD8^+$supp in EC_{B57+} (Fig. 5B5 and extended data Fig.6). In contrast, EC_{B57-} have a higher percentage of $CD8^+$supp (Fig.5A2 and extended data Fig. 6b) expressing less PD1 (Fig. 5B6). EC_{B57-} (EC13) behaves again as an EC_{B57+}. Notably, both subsets are functionally-effective only during adaptive IR and not relevant in the critical earliest days of infection.

Although few immune cell alterations could be detected (Fig. 5C), each EC phenotypic profile was distinct. The majority of these phenotypic alterations, as those found in non-EC, correspond to the direct (HLA-DR, CD38) or indirect (absence of CD26, CD25) effects of IFNα seen in T-cell cultures (extended data Table 1 and extended data Fig. 1). These few but irreversible alterations might occur during the early period of HIV infection in the innate phase of the IR and be augmented by HIV cytopathic effects induced on thymic stromal cells, known to occur during early infection in the innate phase of the IR, and, as reported, also induced by IFNα *(35).*

Discussion

We conclude that besides circulating HIV, the key mediator of AIDS development is elevated circulating IFNα. To be a central major mediator of pathogenesis the criterion should be: active at the earliest days of infection ,ie., in the innate immune phase, be elevated and circulating, and have broad pathogenic effects. IFNα fits these criteria. In non-EC, it is circulating at elevated levels inducing immune cell type abnormalities linked to poor immune cell function (Fig. 1-5 and Table 1). Correspondingly, in EC the absence of circulating high levels IFNα is associated with minimal immune cell types anomalies.We propose that EC avoid the pathogenic vicious circle of high HIV → high IFNα → more HIV → pathogenic IFNα. These assumptions were based on documented experimental data, as follows:

1) <u>At the onset of infection, the critical role played by NK-cells of EC but not non-EC.</u> These cells lyse target cells prior to the viral setpoint. Thus the NK-cells are likely the most effective immune factor reducing viral load and correlated IFNα levels at the onset. Differences between NK-cells from EC and non-EC (Extended data Fig. 7) reside in their functional capacity. Non-EC NK-cells expressing multiple inhibitory receptors including iKIR and checkpoint receptors such as PD1, are likely not functional (Fig. 2B3-4, Table 1). Moreover the low expression of iKIR in NK-cells from EC_{B57+} enables these unaltered cells to lyse infected $CD4^+$T-cells expressing HLA_{B57} restricted HIV epitopes, whereas EC_{B57-} NK-cells expressing iKIR (Fig. 5B1-2), compensate this inhibitory signal by expressing the activating NKG2C receptor (Fig. 5B3) enabling lysis of HLA-E-restricted infected $CD4^+$T-cells.

2) <u>The IFNα-induced impairment of IL-7-induced immune cell homeostasis found in non-EC</u> results in reduction of NK-cells and $CCR7^+CD4^+$ and $CD8^+$T-cells. As a consequence, populations of helper and cytotoxic T-cells are reduced during the later adaptive IR.

3) The hampered IFNα-induced initiation of adaptive IR in non-EC results in diminished $CD4^+$ T-cells activation and proliferation (extended data Table 1).

4) In non-EC, inhibition of CTL and $CD8^+$supp function linked to IFNα-induced inhibitory checkpoints results in loss of control of viral replication (Fig.4 and extended data Table 1).

Concerning the possible immune mechanism enabling control of HIV replication possessed by EC postulated by the AAC *(2)* (Fig. 5), we found that in addition to our hypothesis of a putative lower infectious inoculum, each EC possessed one or more distinct immune mechanisms (Table 1) which could contribute to their avoidance of elevated IFNα levels. These mechanisms include early lysis of infected $CD4^+$T-cells by phenotypically-unaltered NK-cells and additionally during the adaptive IR by cytotoxic CTLs and $CD8^+$supp. These data prompted us to consider that the EC status does not solely depend on one specific genetic and/or immune cell profile but also on a distinct immune capacity, peculiar to each EC and likely additional circumstantial factors such as an inoculum low size. No doubt that the HLA presentation of HIV-peptides by infected cells, including the known HLA_{B57+} but also HLA-E are early contributing factors for NK lysis and, following the adaptive IR for CTL or $CD8^+$supp T-cells. It is also clear that HLA_{B57} genotype is insufficient to account for the EC status, since not all EC are HLA_{B57+} and further HLA_{B57+} is also present in up to 11 percentage of patients with progressive disease, a percentage similar to the uninfected Caucasian population *(4)*. As reported by Altfled et al *(36),* we also suggest that evasion from cytotoxic NK-cell mediated IR by HIV is far more deleterious for early control of viral replication than CTL and $CD8^+$supp, effective only during the adaptive IR. Considering that many immune mechanisms disrupted by HIV due to elevated IFNα in non-EC are avoided by EC (Table 1), we propose that a fortuitous low infectious inoculum is an important contributor to the EC status. This hypothesis has several predictions now under analysis.

This study showed by a comprehensive characterization of the pathogenic levels of IFNα during both anti-HIV innate and adaptive immune reaction : 1) how our data identified elevated IFNα as the key mediator used by HIV to block immune cell attack in non-EC, and 2) why EC, by avoiding this production of elevated IFNα, naturally block HIV replication. Thus, these studies suggest that reducing IFNα production by any acceptable and efficient means could convert non-EC to EC. This proposal is further supported by the experiment carried out on HIV-infected humanized mice showing that anti-IFNα treatment reduced HIV proviral DNA by 14-fold in spleen cells and by 7-fold in bone marrow cells *(27).* In an accompanying manuscript, we will describe the mechanism for the IFNα inefficient anti-HIV IR promoting its progressive elevation.

Online Methods

Human samples. HD were obtained through Etablissement Français du Sang (EFS, Paris, France). 67 people living with HIV were recruited and subdivided into three group: EC (n=18) were obtained from the NVS cohort (Baltimore), non-EC (n=27) were obtained from NIH (Bethesda n=19) and from the Laboratoire de Référence SIDA (Liège n=11). Patient groups did not significantly differ in terms of age, gender, disease status. All participants or their surrogates provided informed consent in accordance with protocols approved by the regional ethical research boards and the Declaration of Helsinki. Clinical data are indicated in extended data Table 2.

Sample processing. Peripheral blood and serum were collected into appropriate tubes. PBMCs were isolated by density gradient centrifugation on Ficoll-Hypaque (Pharmacia, St Quentin en Yvelines, France. PBMCs were stored frozen in liquid.

Cells culture. $CD4^+$T-cells were isolated from frozen PBMCs. All $CD4^+$T-cells were positively selected with a $CD4^+$T-cell isolation kit (Miltenyi Biotec, Germany), yielding $CD4^+$T-cell populations at a purity of 96–99%. Purified $CD4^+$T-cells were stimulated as described previously *(28)* with 4 µg/mL plate-bound anti-human CD3 (OKT3) mAb (eBioscience, San Diego, CA) and 4 µg/mL soluble anti-human CD28 (CD28.2) mAb (Becton Dickinson) in presence of Recombinant human IL-2 (Proleukine, Chiron, Amsterdam, 100 U/mL) and recombinant human interferon alpha-2a (Roferon-A) and IFNλ2 (Biotechne, UK) at the indicated dose. After five days culture, CD38 and CD25 expression as well as the frequency of $7AAD^+$ cells were measured by flow cytometry on stimulated $CD4^+$T-cells (Table S4). NK-cells were isolated from PBMCs. NK-cells were negatively selected with the NK-cell isolation kit (Miltenyi Biotec, Germany), yielding NK-cell populations at a purity of 96–99%. NK-cells were stimulated with IL-15 (Miltenyi Biotec, 10 ng/mL), IL-2 (Proleukine, Chiron, Amsterdam 100 U/mL) and recombinant human interferon alpha-2a (Roferon-A) at the indicated dose. After 3 days of culture, expression of CD56, CD95 and NKG2D was measured by flow cytometry (extended data Table 3a).

Flow cytometry analysis.

*MAbs panels, staining***.** Immunophenotypic studies were performed on frozen samples, using up to 23-colours flow cytometry panels. See extender data Table 3 for antibody panel information. The list of mAbs used are detailed in gating strategy we used to identify the immune cell subtypes and their respective subsets are represented in extended data Fig. 3. Antibody titration was performed to choose the concentration that provided the maximal brightness of the positive cell population and the lowest signal for the negative cell population. Approximately 1×10^6 to 5×10^6 frozen PBMCs were used per patient per stain. Staining was performed as described previously *(28)* except for the panel using HLA-E- or HLA-A*02-pentamers (Pro-immune). Pre-incubation with a blocking anti-CD94 mAb (clone

HP-3D9, 5 μg/mL, BD Biosciences) was performed to completely abrogate the non-specific staining of $CD94^+$/$NKG2^+$ T cells by HLA-E-pentamers before the staining with the other antibodies. Cells were acquired on Cytek Aurora flow cytometer. Data were analysed using FlowJo software (FlowJo, LLC). Flow cytometry data were identified as the proportion (%) of cells expressing the marker, and protein levels as MFI. Unsupervised analyses were performed using cytobank software and R studio software.

7-AAD (7-amino-actinomycin D) staining. Apoptosis of stimulated CFD-labeled $CD4^+$T-cells was determined using the 7-AAD assay (1). Briefly, cultured cells were stained with 20 μg/mL nuclear dye 7-AAD (Sigma-Aldrich) for 30 min at 4 °C. FSC/7-AAD dot plots distinguish living (FSC^{high}/7-AAD−) from apoptotic (FSChigh/7-AAD+) cells and apoptotic bodies (FSClow/7- AAD+) and debris ((FSClow/7-AAD−). Living cells were identified as $CD3^+$7-AAD−FSC^+ cells *(37)*.

CellTrace violet staining. $CD4^+$T-cells and NK-cells were stained with 1 μM dye (CellTrace violet; Molecular Probes/Invitrogen) in PBS for 8 min at 37°C at a concentration of 1 X 10^6 cells/mL. The labelling was stopped by washing the cells twice with RPMI-1640 culture medium containing 10% FBS. The cells were then re-suspended at the desired concentration and subsequently used for proliferation assays.

Composite cell phenotypic alteration score. We generate a cumulative phenotypic score for each T-cell subsets. The frequency of the following markers was used to calculate the score: $CD25^-$,$CD26^-$;$HLA\text{-}DR^+$,$CD38^+$, $CTLA\text{-}4^+$,$CD28^-$,$PD1^+$ and $CD39^+$. It is calculated as the sum of the ratio of the expression level of each marker to the average expression level of the corresponding marker in the HD.

Cytokines quantification. Serum IFNα and IFNλ2 levels were determined using Simoa cytokine assays (references 100860 and 101419 respectively). Van der Sluis et al showing that

HIV infection of co-cultures of $CD4^+$T-cells and pDCs enhanced mRNA expression of IFNλ2 and not IFNλ1 or IFNλ3, we focused only on serum IFNλ2 levels (*38*). IL-10 in 4 day-cell culture supernatants was determined by Luminex technology (human custom Procarta Plex, Invitrogen)

Statistical analyses. Statistical significance of differences between groups was assessed using the unpaired nonparametric Mann-Whitney. Non-parametric, paired Wilcoxon tests were used for paired data. Correlations were assessed by the nonparametric Spearman test. Analyses were performed with GraphPad-Prism, and R. Two-sided P value less than .05 was considered statistically significant (ns: nonsignificant; *P < .05; **P < .01; ***P < .001; ****P < .0001).

Acknowledgements :

We thank the study volunteers and medical personnel. We also thank Elissa Miller for her skillful administrative and editorial collaboration and Philip Embiricos for financial support . M.M.S is supported by R01AI147870 and IBX002358A.

Author contributions: R.G., D.Z., and H.L.B. designed research; H.L.B. V.S., M.M, D.B., A.H.-K., and H.S. performed research; H.L.B., V.S., M.M, D.B., A.H.-K., H.S. J.-D.B., A.B, , R.G., and D.Z. analyzed data; S.K., M.S., C.F.L and G.D. provided blood cells and serum samples, clinical data samples from HIV patients and clinical input. H.L.B., R.G., D.Z., wrote the paper. All authors contributed to review and editing and agreed to the published version of the manuscript.

References

1. Deeks, S. G. & Walker, B. D. Human Immunodeficiency Virus Controllers: Mechanisms of Durable Virus Control in the Absence of Antiretroviral Therapy. *Immunity* **27**, 406–416 (2007).

2. Jiang, C. *et al.* Distinct viral reservoirs in individuals with spontaneous control of HIV-1. *Nature* **585**, 261–267 (2020).

3. Martin, M. P. *et al.* Innate partnership of HLA-B and KIR3DL1 subtypes against HIV-1. *Nat. Genet.* **39**, 733–740 (2007).

4. Migueles, S. A. *et al.* HLA B*5701 is highly associated with restriction of virus replication in a subgroup of HIV-infected long term nonprogressors. *Proc. Natl. Acad. Sci.* **97**, 2709–2714 (2000).

5. Zagury, D. *et al.* Interferon alpha and Tat involvement in the immunosuppression of uninfected T cells and C-C chemokine decline in AIDS. *Proc. Natl. Acad. Sci. U. S. A.* **95**, 3851–3856 (1998).

6. Gringeri, A. *et al.* A randomized, placebo-controlled, blind anti-AIDS clinical trial: safety and immunogenicity of a specific anti-IFN alpha immunization. *J. Acquir. Immune Defic. Syndr.* **7**, 978–988 (1994).

7. Cha, L., de Jong, E., French, M. A. & Fernandez, S. IFN-α Exerts Opposing Effects on Activation-Induced and IL-7–Induced Proliferation of T Cells That May Impair Homeostatic Maintenance of CD4 $^{+}$ T Cell Numbers in Treated HIV Infection. *J. Immunol.* **193**, 2178–2186 (2014).

8. Dondi, E., Rogge, L., Lutfalla, G., Uzé, G. & Pellegrini, S. Down-modulation of responses to type I IFN upon T cell activation. *J. Immunol. Baltim. Md 1950* **170**, 749–756 (2003).

9. Aman, M. *et al.* Interferon-alpha stimulates production of interleukin-10 in activated CD4+ T cells and monocytes. *Blood* **87**, 4731–4736 (1996).

10. Le Buanec, H. *et al.* IFN- and CD46 stimulation are associated with active lupus and skew natural T regulatory cell differentiation to type 1 regulatory T (Tr1) cells. *Proc. Natl. Acad. Sci.* **108**, 18995–19000 (2011).

11. Friedman, R. L., Manly, S. P., McMahon, M., Kerr, I. M. & Stark, G. R. Transcriptional and posttranscriptional regulation of interferon-induced gene expression in human cells. *Cell* **38**, 745–755 (1984).

12. Lazear, H. M., Schoggins, J. W. & Diamond, M. S. Shared and Distinct Functions of Type I and Type III Interferons. *Immunity* **50**, 907–923 (2019).

13. Reis, G. *et al.* Early Treatment with Pegylated Interferon Lambda for Covid-19. *N. Engl. J. Med.* **388**, 518–528 (2023).

14. Anokhin, V. V. *et al.* Previously Unidentified Single Nucleotide Polymorphisms in HIV/AIDS Cases Associate with Clinical Parameters and Disease Progression. *BioMed Res. Int.* **2016**, 2742648 (2016).

15. Jacquelin, B. *et al.* Nonpathogenic SIV infection of African green monkeys induces a strong but rapidly controlled type I IFN response. *J. Clin. Invest.* JCI40093 (2009) doi:10.1172/JCI40093.

16. Harris, L. D. *et al.* Downregulation of Robust Acute Type I Interferon Responses Distinguishes Nonpathogenic Simian Immunodeficiency Virus (SIV) Infection of Natural Hosts from Pathogenic SIV Infection of Rhesus Macaques. *J. Virol.* **84**, 7886–7891 (2010).

17. Gringeri, A. *et al.* Active anti-interferon-alpha immunization: a European-Israeli, randomized, double-blind, placebo-controlled clinical trial in 242 HIV-1--infected patients (the EURIS study). *J. Acquir. Immune Defic. Syndr. Hum. Retrovirology Off. Publ. Int. Retrovirology Assoc.* **20**, 358–370 (1999).

18. Wherry, E. J. T cell exhaustion. *Nat. Immunol.* **12**, 492–499 (2011).

19. Du, J. *et al.* Persistent High Percentage of HLA-DR+CD38high CD8+ T Cells Associated With Immune Disorder and Disease Severity of COVID-19. *Front. Immunol.* **12**, 735125 (2021).

20. Huang, Y. *et al.* Inhibition of the adenosinergic pathway: the indispensable part of oncological therapy in the future. *Purinergic Signal.* **15**, 53–67 (2019).

21. Jiang, H. & Chess, L. The specific regulation of immune responses by CD8+ T cells restricted by the MHC class Ib molecule, Qa-1. *Annu. Rev. Immunol.* **18**, 185–216 (2000).

22. Marijt, K. A., Doorduijn, E. M. & van Hall, T. TEIPP antigens for T-cell based immunotherapy of immune-edited HLA class Ilow cancers. *Mol. Immunol.* **113**, 43–49 (2019).

23. Joosten, S. A., Sullivan, L. C. & Ottenhoff, T. H. M. Characteristics of HLA-E Restricted T-Cell Responses and Their Role in Infectious Diseases. *J. Immunol. Res.* **2016**, 1–11 (2016).

24. Poli, A. *et al.* CD56 ^{bright} natural killer (NK) cells: an important NK cell subset. *Immunology* **126**, 458–465 (2009).

25. Alter, G. *et al.* Sequential deregulation of NK cell subset distribution and function starting in acute HIV-1 infection. *Blood* **106**, 3366–3369 (2005).

26. Soumelis, V. *et al.* Depletion of circulating natural type 1 interferon-producing cells in HIV-infected AIDS patients. *Blood* **98**, 906–912 (2001).

27. Cheng, L. *et al.* Blocking type I interferon signaling enhances T cell recovery and reduces HIV-1 reservoirs. *J. Clin. Invest.* **127**, 269–279 (2016).

28. Schiavon, V. *et al.* Microenvironment tailors nTreg structure and function. *Proc. Natl. Acad. Sci.* **116**, 6298–6307 (2019).

29. Sallusto, F., Lenig, D., Förster, R., Lipp, M. & Lanzavecchia, A. Two subsets of memory T lymphocytes with distinct homing potentials and effector functions. *Nature* **401**, 708–712 (1999).

30. Stacey, A. R. *et al.* Induction of a Striking Systemic Cytokine Cascade prior to Peak Viremia in Acute Human Immunodeficiency Virus Type 1 Infection, in Contrast to More Modest and Delayed Responses in Acute Hepatitis B and C Virus Infections. *J. Virol.* **83**, 3719–3733 (2009).

31. Schwartz, O., Maréchal, V., Le Gall, S., Lemonnier, F. & Heard, J. M. Endocytosis of major histocompatibility complex class I molecules is induced by the HIV-1 Nef protein. *Nat. Med.* **2**, 338–342 (1996).

32. Sallusto, F., Geginat, J. & Lanzavecchia, A. Central memory and effector memory T cell subsets: function, generation, and maintenance. *Annu. Rev. Immunol.* **22**, 745–763 (2004).

33. Kim, H.-J. *et al.* CD8 $^{+}$ T regulatory cells express the Ly49 Class I MHC receptor and are defective in autoimmune prone B6-Yaa mice. *Proc. Natl. Acad. Sci.* **108**, 2010–2015 (2011).

34. Li, J. *et al.* KIR+CD8+ T cells suppress pathogenic T cells and are active in autoimmune diseases and COVID-19. *Science* **376**, eabi9591 (2022).

35. Dutrieux, J. *et al.* Modified interferon-α subtypes production and chemokine networks in the thymus during acute simian immunodeficiency virus infection, impact on thymopoiesis. *AIDS Lond. Engl.* **28**, 1101–1113 (2014).

36. Altfeld, M. & Goulder, P. 'Unleashed' natural killers hinder HIV. *Nat. Genet.* **39**, 708–710 (2007).

37. Lecoeur, H., de Oliveira-Pinto, L. M. & Gougeon, M.-L. Multiparametric flow cytometric analysis of biochemical and functional events associated with apoptosis and oncosis using the 7-aminoactinomycin D assay. *J. Immunol. Methods* **265**, 81–96 (2002).

38. Van der Sluis, R. M. *et al.* Diverse effects of interferon alpha on the establishment and reversal of HIV latency. *PLoS Pathog.* **16**, e1008151 (2020).

39. Nguyen, T. P. *et al.* Interferon- *α* inhibits CD4 T cell responses to interleukin-7 and interleukin-2 and selectively interferes with Akt signaling. *J. Leukoc. Biol.* **97**, 1139–1146 (2015).

40. Dondi, E., Rogge, L., Lutfalla, G., Uzé, G. & Pellegrini, S. Down-modulation of responses to type I IFN upon T cell activation. *J. Immunol. Baltim. Md 1950* **170**, 749–756 (2003).

41. Boasso, A., Hardy, A. W., Anderson, S. A., Dolan, M. J. & Shearer, G. M. HIV-Induced Type I Interferon and Tryptophan Catabolism Drive T Cell Dysfunction Despite Phenotypic Activation. *PLoS ONE* **3**, e2961 (2008).

42. Guo, K. *et al.* Qualitative Differences Between the IFNα subtypes and IFNβ Influence Chronic Mucosal HIV-1 Pathogenesis. *PLOS Pathog.* **16**, e1008986 (2020).

43. Zhen, A. *et al.* Targeting type I interferon-mediated activation restores immune function in chronic HIV infection. *J. Clin. Invest.* **127**, 260–268 (2017).

44. Cheng, L. *et al.* Blocking type I interferon signaling enhances T cell recovery and reduces HIV-1 reservoirs. *J. Clin. Invest.* **127**, 269–279 (2017).

45. Terawaki, S. *et al.* IFN-α directly promotes programmed cell death-1 transcription and limits the duration of T cell-mediated immunity. *J. Immunol. Baltim. Md 1950* **186**, 2772–2779 (2011).

46. Hafler, D. *et al.* Type I Interferon Transcriptional Network Regulates Expression of Coinhibitory Receptors in Human T cells. *Res. Sq.* rs.3.rs-133494 (2021) doi:10.21203/rs.3.rs-133494/v1.

47. Zella, D. *et al.* IFN-alpha 2b reduces IL-2 production and IL-2 receptor function in primary CD4+ T cells. *J. Immunol. Baltim. Md 1950* **164**, 2296–2302 (2000).

48. Lanna, A. *et al.* IFN-α inhibits telomerase in human CD8^{+} T cells by both hTERT downregulation and induction of p38 MAPK signaling. *J. Immunol. Baltim. Md 1950* **191**, 3744–3752 (2013).

49. Ng, C. T. & Oldstone, M. B. A. Infected CD8α- dendritic cells are the predominant source of IL-10 during establishment of persistent viral infection. *Proc. Natl. Acad. Sci. U. S. A.* **109**, 14116–14121 (2012).

50. Bazhin, A. V., von Ahn, K., Fritz, J., Werner, J. & Karakhanova, S. Interferon-α Up-Regulates the Expression of PD-L1 Molecules on Immune Cells Through STAT3 and p38 Signaling. *Front. Immunol.* **9**, 2129 (2018).

51. Kaser, A., Nagata, S. & Tilg, H. Interferon alpha augments activation-induced T cell death by upregulation of Fas (CD95/APO-1) and Fas ligand expression. *Cytokine* **11**, 736–743 (1999).

52. Fraietta, J. A. *et al.* Type I interferon upregulates Bak and contributes to T cell loss during human immunodeficiency virus (HIV) infection. *PLoS Pathog.* **9**, e1003658 (2013).

53. Herbeuval, J.-P. *et al.* Regulation of TNF-related apoptosis-inducing ligand on primary CD4+ T cells by HIV-1: role of type I IFN-producing plasmacytoid dendritic cells. *Proc. Natl. Acad. Sci. U. S. A.* **102**, 13974–13979 (2005).

54. Wilson, E. B. *et al.* Emergence of distinct multiarmed immunoregulatory antigen-presenting cells during persistent viral infection. *Cell Host Microbe* **11**, 481–491 (2012).

55. Swiecki, M. *et al.* Type I interferon negatively controls plasmacytoid dendritic cell numbers in vivo. *J. Exp. Med.* **208**, 2367–2374 (2011).

56. Anz, D. *et al.* Activation of melanoma differentiation-associated gene 5 causes rapid involution of the thymus. *J. Immunol. Baltim. Md 1950* **182**, 6044–6050 (2009).

57. Alvarez, M. D. L. *et al.* Cross-talk between IFN-alpha and TGF-beta1 signaling pathways in preneoplastic rat liver. *Growth Factors Chur Switz.* **27**, 1–11 (2009).

Table 1: Contribution of immune mechanisms to the Elite Controler status

	Sample	VL	CD4 count (copies/ml)	IFNα (fg/ml)	IFNλ (fg/ml)	pDC (%)	$CD8^+$ CM (%)	CTL $PD1^-$ (%) ◆	$CD8^+$ supp $PD1^-$ (%) ◆	Mature NK $NKG2C^+$ (%) ◆	Mature NK $iKIR^-$ (%) ◆	Mature NK $iKIR^+$ $PD1^-$ (%) ◆	Loss of EC status (indication)
B57-	EC 47	<20	891	3.37	171.96	NA	5.7	37.75	23.15	11.7	26.8	72.72	
	EC 58	59	1745	5.58	2389.62	13.9	6.04	35.36	22.62	26.5	37.1	62.14	
	EC 13	<40	864	6.45	257.48	58.7	13.5	55.07	4.51	33.8	66.8	32.91	
	EC 32	<48	643	7.66	319.75	NA	NA	NA	NA	NA	NA	NA	
	EC 31*	<48	587	67.31	500.06	28.6	3.86	47.04	32.25	23.4	38.7	59.59	Volunteer for cART treatment
	EC 55	50	482	72.21	578.54	NA	6.91	29.93	30.19	23.5	27.7	72.06	
	EC 3	334	1140	74.43	766.29	NA	0.77	44.41	21.57	25.9	46.2	53.41	
B57+	EC 63	<40	632	0	338.45	50.4	27.7	61.37	8.86	17	55.8	43.85	
	EC 9	<40	496	0	182.96	9.98	16.7	33.33	2.83	7.79	74.4	25.30	
	EC 65*	<48	1792	0.75	308.57	37.9	9.25	57.82	14.41	19.4	20.3	78.37	Volunteer for cART treatment
	EC 6	<75	1889	8.48	1875.86	11.5	21.7	46.04	7.91	12.8	61.2	38.60	
	EC 42	<220	731	12.44	142.63	35.9	10.4	42.67	20.62	14.7	44.7	52.04	
	EC 51	<40	1250	18.1	32441.4	51.3	9.39	53.55	8.61	9.14	54.5	45.34	
	EC 4	<40	952	25.28	774.38	8.17	9.37	25.74	5.94	5.61	47.2	52.54	
	EC 8*	<40	1018	57.14	2873.66	36.9	10.1	46.45	8.23	4.89	66.8	32.96	Colon carcinoma
	EC 11^+	<40	917	348.08	1639.51	7.29	13.9	17.16	0.95	9.14	41.3	51.48	Hepatitis C
	EC 52^+	<20	340	796.94	2384.02	NA	6.85	38.43	13.71	12.6	41.7	57.82	Hepatitis C
	EC 68^+	169	584	99.63	830.17	NA	NA	NA	NA	NA	NA	NA	last VL = 1380 cp/ml
B57- (med) n=7		59	864	7.66	500.06	28.6	5.87	41.08	22.88	24.7	37.9	60.86	
B57+ (med) n=11		<40	917	18.1	830.17	35.9	10.25	44.36	8.42	10.87	50.85	48.41	
non EC (med) n=26		21701	404.5	93.01	1027.92	13.7	4.155	42.90	19.12	28.85	36.4	59.60	
HD (med) n=65		NA	NA	17.72	595.35	26.7	9.92	41.47	20.27	4.14	50.95	48.85	
EC (med) n=18		114	877.5	15.27	672.415	32.25	9.38	43.54	11.29	13.75	45.45	52.29	

The table details enhanced or diminished immune mechanisms contributing to the EC status found in EC individuals more elevated than in non-EC

1) Three patients lost their EC status: EC 31 and EC 65 volunteer for cART treatment trial, and EC8 for colonic carcinoma complications (*)

2) Three individuals (EC11, EC52 and EC68,) have a serum IFNα over the non-EC median (+)

3) Note that cytotoxic NK-cells, CTL and $CD8^+$supp in non-EC are phenotypically hampered (◆)

Figures legends

Figure 1: Comparative analysis of major blood immune cell subsets and serum IFNα and IFNλ2 concentration in non-EC, EC and HD.

(A) Principal component analysis (PCA) of studied participants based on the proportion of different immune cell subpopulations ($CD4^+$, $CD8^+$ and TCR γδ T-cells, NK and DC), evaluated by flow cytometry. Immune cell profiling was assessed by flow cytometry as depicted in extended data Fig. 3. The first two Principal components (PC1 and PC2) explaining the greatest differences among individuals are represented on a bi-plot. Each point represents one participant, colored by the group they belong to. Each group is outlined by an ellipse representing the 95% confidence interval of the sample groupings. (**B**) Histograms showing distributions of indicated immune cell populations between HD (Black, n=24), EC (green, n=16), and non-EC (red, n=26). (**C**) Balloon-plot summarizing the statistically significant changes in the indicated immune cell populations between EC and HD, non-EC and HD and non-EC and EC. The size of the circle represents the p-value. Red and blue colors show increased or decreased frequencies of the immune cell populations. (**D**) Scatterplots showing IFNα and IFNλ2 concentration in serum from HD (n=51), EC (n=18) and non-EC (n=26). IFNα and IFNλ2 levels were detected by SIMOA. (**E**) Scatterplot showing relationships between IFNα and IFNλ2 serum levels (**E1**), $CD4^+$T-cells and IFNλ2 (**E2**), and $CD8^+$T-cells and IFNλ2 (**E3**) in EC (n=18) and non-EC (n=26). Correlations were evaluated with Spearman's rank correlation test. Differences between unpaired samples were performed with Mann-Whitney test. Graph show the median values and p values (*P<0.05, **P<0.01, ***P<0.001, ****P<0.0001)

Figure 2: Comparative distribution and immune phenotypic analysis of innate immune NK-cells in HD, EC and non-EC. (**A1**) SPADE tree showing the distribution of the three main NK-cell subsets in HD, EC and non-EC, based on CD56 and CD16 expression levels. Nodes are colored by count. (**A2**) Representative Flow Cytometry plots of NK-cell subsets gated on $CD19^{-}CD14^{-}TCR\gamma\delta^{-}CD3^{-}HLA\text{-}DR^{-}$ cells from the 3 studied groups: early NK ($CD56^{bright}/CD16^{-}$), mature NK ($CD56^{dim}/CD16^{+}$) and terminal NK ($CD56^{-}CD16^{+}$). (**A3**) Frequency of early, mature and terminal NK in each studied group (HD n=22, EC n=12 and non-EC n=8). Profiles displaying the expression level of Helios, NCR (NKp30, NKp44, NKp46), GrzB/perf (**B1)** and CD26, CD39, iKIR (**B3)** on mature NK-cells from HD (black), EC (green) and non-EC (red). (**B2** and **B4**) Box plots displaying the frequency of the indicated markers in mature NK-cells in each studied group. (**C**) Scatterplots showing relationships between IFNα serum level and the frequencies of selected NK-cell subsets. Correlations were evaluated with Spearman's rank correlation test. Histograms showing the expression level (measured by median fluorescence intensity (MFI) of NKGD2 in early NK-cells (**D1**) and CD95 in mature NK-cells (**D2**) in non-EC (n=6) and HD (n=5). Percentage of viable NK-cells (**E1**) and frequency of CFD^{low} NK-cells (**E2**) after 7 days of culture in presence of increasing doses of IFNα. Histograms showing the expression level of CD56 in $CD56^{dim/neg}$ NK-cells (**E3**), distribution of mature (grey) and terminal NK-cells (black) (**E4**), expression levels of NKG2D in early NK-cells (**E5**) and CD95 in mature NK-cells (**E6**) after 3 days of culture in presence of IFNα. Significance was determined by unpaired Mann-Whitney U test. *P<0.05, **P<0.01, ***P<0.001, ****P<0.0001.

Figure 3: Comparative immune phenotypic analysis of (A) CD4$^+$Tconv, CD19$^+$B-cells and (B) CD4$^+$Treg in non-EC, EC, and HD.

(**A1**) SPADE tree showing the distribution of CD4$^+$Tconv subsets in HD, EC and non-EC. Nodes are colored by count. CD4$^+$Tconv can be classified into four major subsets by their expression of CD45RA and the chemokine receptor CCR7: naïve (CCR7$^+$CD45RA$^+$); CM (CCR7$^+$CD45RA$^-$), EM (CCR7$^-$CD45RA$^-$) and TEMRA (CCR7$^-$CD45RA$^+$). (**A2**) Frequency of Naïve, CM, EM and TEMRA in each studied group (HD n=24, EC n=16 and non-EC n=23). Boxplots showing the expression of indicated marker in CD4$^+$ CM (**A3**) across the groups (HD n=22, EC n=12 and non-EC n=8). (**A4**) Radar chart showing a composite score of phenotypic cell alteration calculated for each CD4$^+$Tconv subpopulation in non-EC and EC (see Methods). Frequency of cTfh (**A5a**), expression levels of CXCR5 in cTfh (**A5b**) and frequency of cTfh co-expressing CD38 and HLADR (**A5c**) in non-EC (n=6) and HD (n=5). Proportion of CD19$^+$ B-cells (**A6a**), frequency (**A6b**) and expression level (**A6c**) of CXCR5 in CD19$^+$B-cells in non-EC (n=6) and HD (n=5). (**B1**) Representative flow cytometry plots of CD25$^+$Foxp3$^+$ cells within CD4$^+$T-cells isolated from HD, EC and non-EC. (**B2**) Histograms showing the frequency of Foxp3 in CD4$^+$T-cells, (**B3**) histograms displaying the CD25 expression level in CD4$^+$ Foxp3$^+$T-cells and **(B4)** the Treg CD25$^-$ variant frequency in CD4$^+$Foxp3 T-cells in each studied group. **(B5)** Scatterplots showing relationships between frequency of Treg CD25$^-$ variant in HIV-infected patients and serum IFNα levels. (**B6**) Proportion of specific functional signaling checkpoint on memory CD4$^+$ Treg (CD4$^+$ Foxp3$^+$CD25$^+$CD45RA$^-$) of each studied group (HD n=22, EC n=12 and non-EC n=8). Correlations were evaluated using Spearman's rank correlation test. Significance was determined by unpaired Mann-Whitney U test. *P<0.05, **P<0.01, ***P<0.001, ****P<0.0001.

Figure 4: Comparative immune phenotypic analysis of CD8$^+$T-cell subsets in non-EC, EC and HD.

(**A1**) Representative viSNE plot showing the distribution CD8$^+$T-cell subsets, as described above for CD4$^+$Tconv in HD, EC, and non-EC. (**A2**) Histograms showing the frequency of Naïve, CM, EM and TEMRA CD8$^+$T-cells subsets in each studied group (HD n=24, EC n=16 and non-EC n=23). Boxplots showing the expression of indicated marker in CD8$^+$CM (**A3**) and TEMRA (**A4**) across the groups (HD n=22, EC n=12 and non-EC n=8). (**A5**) Radar chart showing a composite score of phenotypic cell alteration calculated for each CD8$^+$T-cell subpopulations in EC and non-EC (EC n=12 and non-EC n=8). (**A6**) Scatterplots showing relationships between the expression level of indicated markers in CD8$^+$CM (EC n=12 and non-EC n=8). (**B**) ViSNE plot depicting the phenotypic difference between CD8$^+$CTL (TEMRA iKIR$^-$) (**B1**) and CD8$^+$supp (TEMRA iKIR$^+$) (**B2**). tSNE plot of CD8$^+$T-cell subsets showed in different colors and viSNE projections of expression of indicated markers are shown. Red and black arrows indicate HLA-1a restricted and HLA-E-restricted CD8$^+$supp respectively. Histograms showing the frequency of CD8$^+$TEMRA iKIR$^-$ (**B3**) and TEMRA iKIR$^+$ (**B4**) in each studied group (HD n=24, EC n=16 and non-EC n=26). Box plots showing the proportion of specific markers on CD8$^+$TEMRA iKIR$^-$ (**B5**) and TEMRA iKIR$^+$ (**B6**) in each studied group (HD n=22, EC n=12 and non-EC n=8). Correlations were evaluated using Spearman's rank correlation test. Significance was determined by unpaired Mann-Whitney U test. *P<0.05, **P<0.01, ***P<0.001, ****P<0.0001.

Figure 5: Distinct immune cells phenotypic patterns between non-B57 and B57 EC with a peculiar profile displayed by each patient of these subgroups.

(**A1**) PCA scatterplots of $CD8^+$T-cell subpopulations frequencies for non-B57 (EC_{B57-}) and B57 (EC_{B57+}) EC (shown as blue and green dots respectively). (**A2**) Heatmaps representing the distribution of the indicated lymphocytes subsets in EC. Histograms showing frequency and index ratio of indicated subsets in mature NK (**B1-3**) and $CD8^+$T-cell compartment (**B4-6**). (**C**) Heatmaps showing the frequency of indicated markers in $CD4^+$ Treg, $CD4^+$CM, $CD8^+$CM, $CD8^+$CTL, $CD8^+$supp and mature NK-cells.

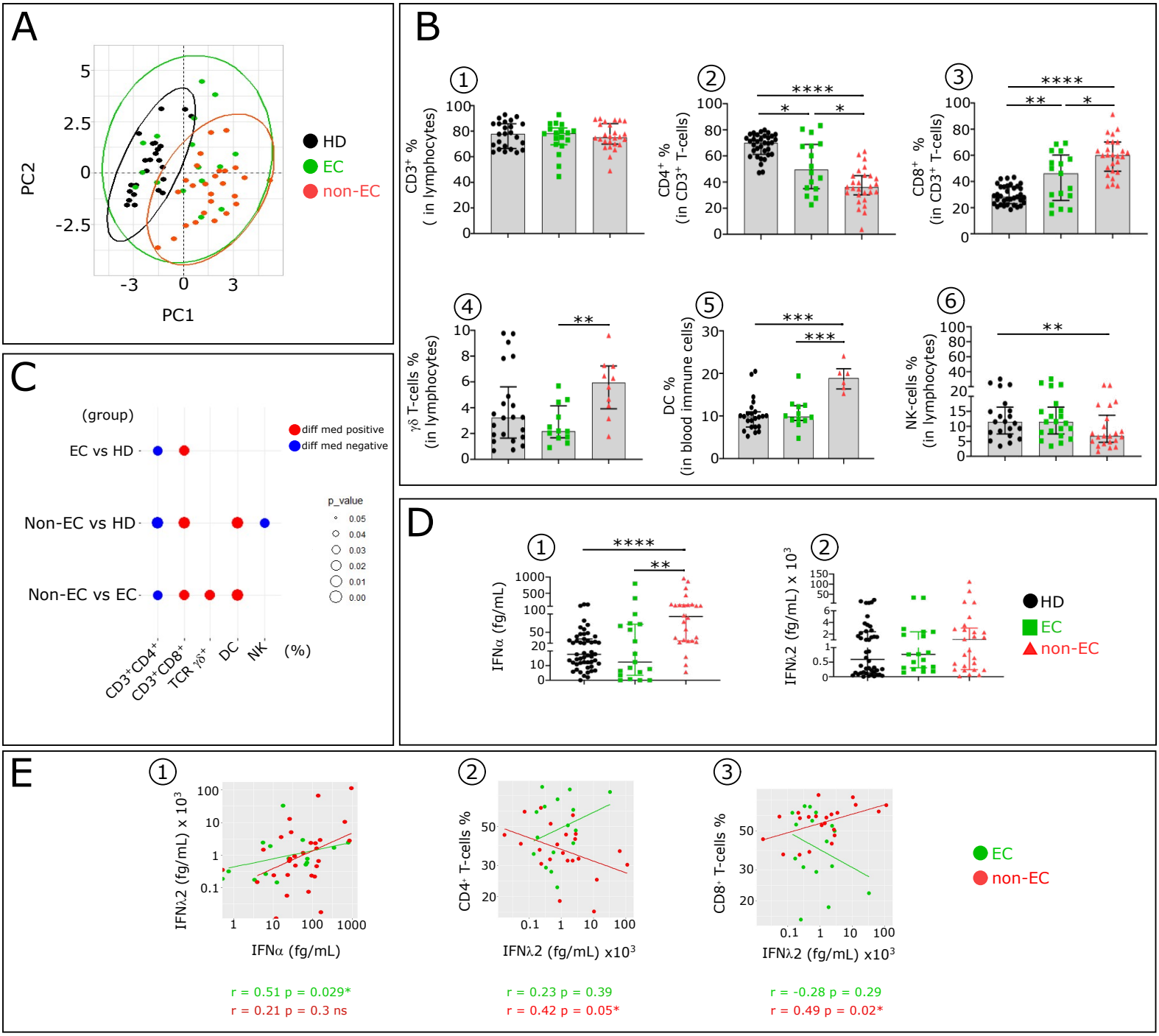
A
PC2
PC1
HD
EC
non-EC
B
CD3+ % (in lymphocytes)
CD4+ % (in CD3+ T-cells)
CD8+ % (in CD3+ T-cells)
γδ T-cells % (in lymphocytes)
DC % (in blood immune cells)
NK-cells % (in lymphocytes)
C
(group)
diff med positive
diff med negative
EC vs HD
Non-EC vs HD
Non-EC vs EC
p_value
CD3+CD4+
CD3+CD8+
TCR γδ+
DC
NK
(%)
D
IFNα (fg/mL)
IFNλ2 (fg/mL) x 10³
HD
EC
non-EC
E
IFNλ2 (fg/mL) x 10³
IFNα (fg/mL)
CD4+ T-cells %
IFNλ2 (fg/mL) x10³
CD8+ T-cells %
IFNλ2 (fg/mL) x10³
EC
non-EC
r = 0.51 p = 0.029*
r = 0.21 p = 0.3 ns
r = 0.23 p = 0.39
r = 0.42 p = 0.05*
r = -0.28 p = 0.29
r = 0.49 p = 0.02*

Figure 1

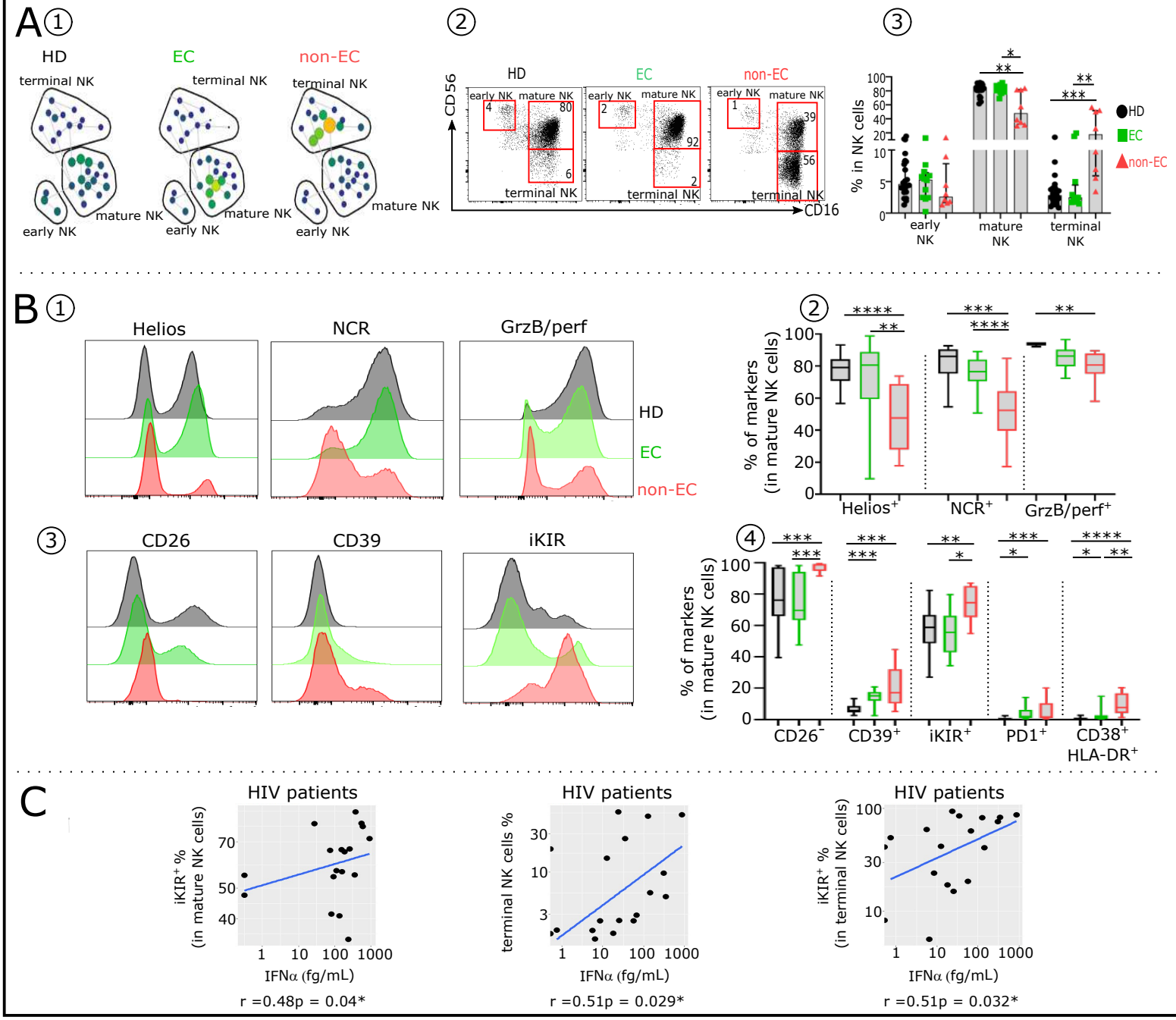
A
HD
EC
non-EC
terminal NK
mature NK
early NK
CD56
CD16
% in NK cells
B
Helios
NCR
GrzB/perf
CD26
CD39
iKIR
% of markers (in mature NK cells)
Helios+
NCR+
GrzB/perf+
CD26−
CD39+
iKIR+
PD1+
CD38+ HLA-DR+
C
HIV patients
iKIR+ % (in mature NK cells)
terminal NK cells %
iKIR+ % (in terminal NK cells)
IFNα (fg/mL)
r =0.48p = 0.04*
r =0.51p = 0.029*
r =0.51p = 0.032*
D
NKG2D MFI (in early NK NKG2D positive cells)
CD95 MFI (in mature NK CD95 positive cells)
E
viability (%)
CD56 MFI (in CD56dim/neg)
NKG2D MFI (in early NK cells)
% of CFDlow (in NK cells)
% of cells
CD95 MFI (in mature NK cells)

Figure 2

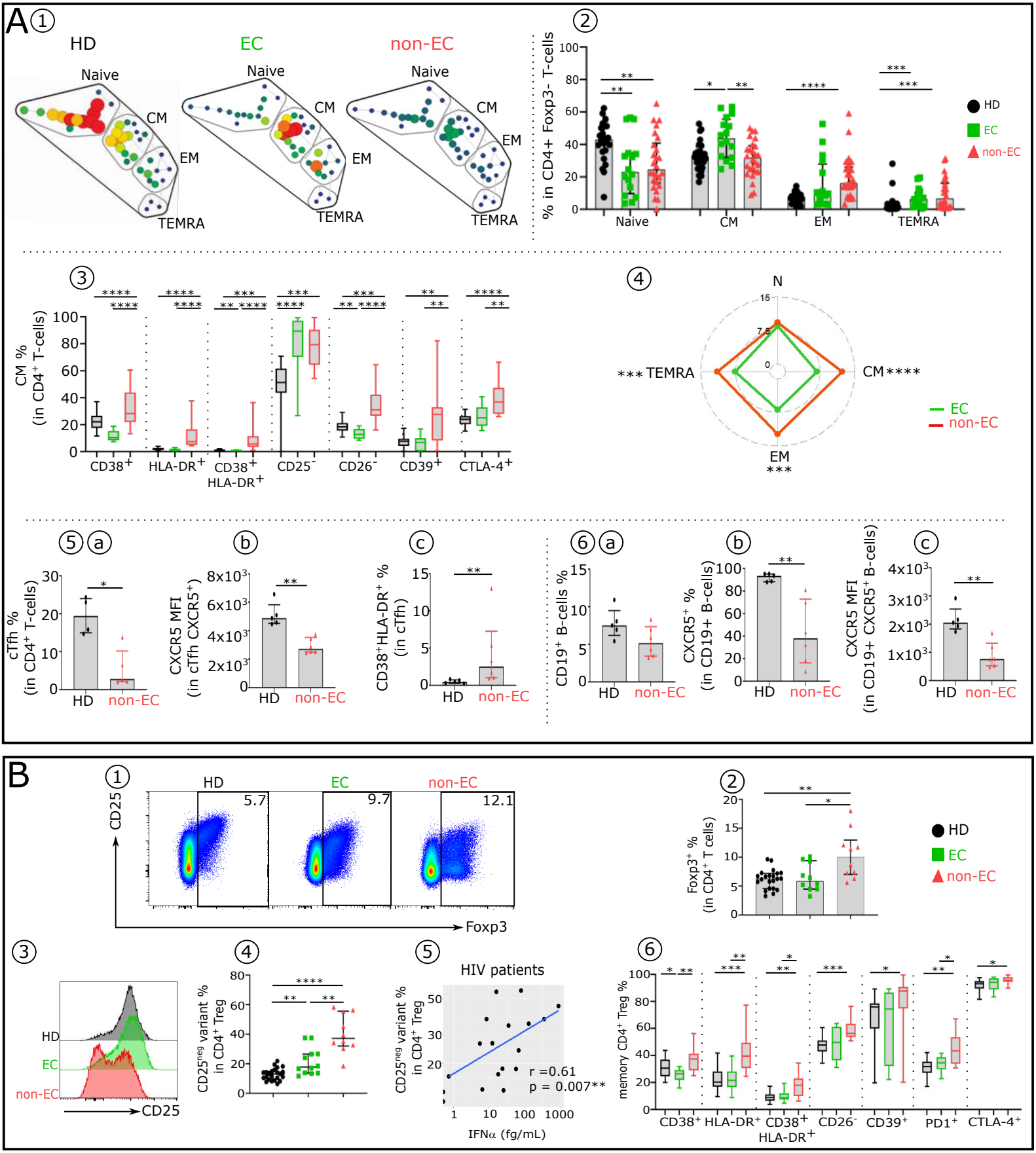
A
HD
EC
non-EC
Naive
CM
EM
TEMRA
% in CD4+ Foxp3- T-cells
HD
EC
non-EC
CM % (in CD4+ T-cells)
CD38+
HLA-DR+
CD38+ HLA-DR+
CD25-
CD26-
CD39+
CTLA-4+
N
TEMRA
CM
EM
cTfh % (in CD4+ T-cells)
CXCR5 MFI (in cTfh CXCR5+)
CD38+HLA-DR+ % (in cTfh)
CD19+ B-cells %
CXCR5+ % (in CD19+ B-cells)
CXCR5 MFI (in CD19+ CXCR5+ B-cells)
B
CD25
Foxp3
5.7
9.7
12.1
Foxp3+ % (in CD4+ T cells)
CD25
CD25neg variant % in CD4+ Treg
HIV patients
r =0.61
p = 0.007**
IFNα (fg/mL)
memory CD4+ Treg %
PD1+

Figure 3

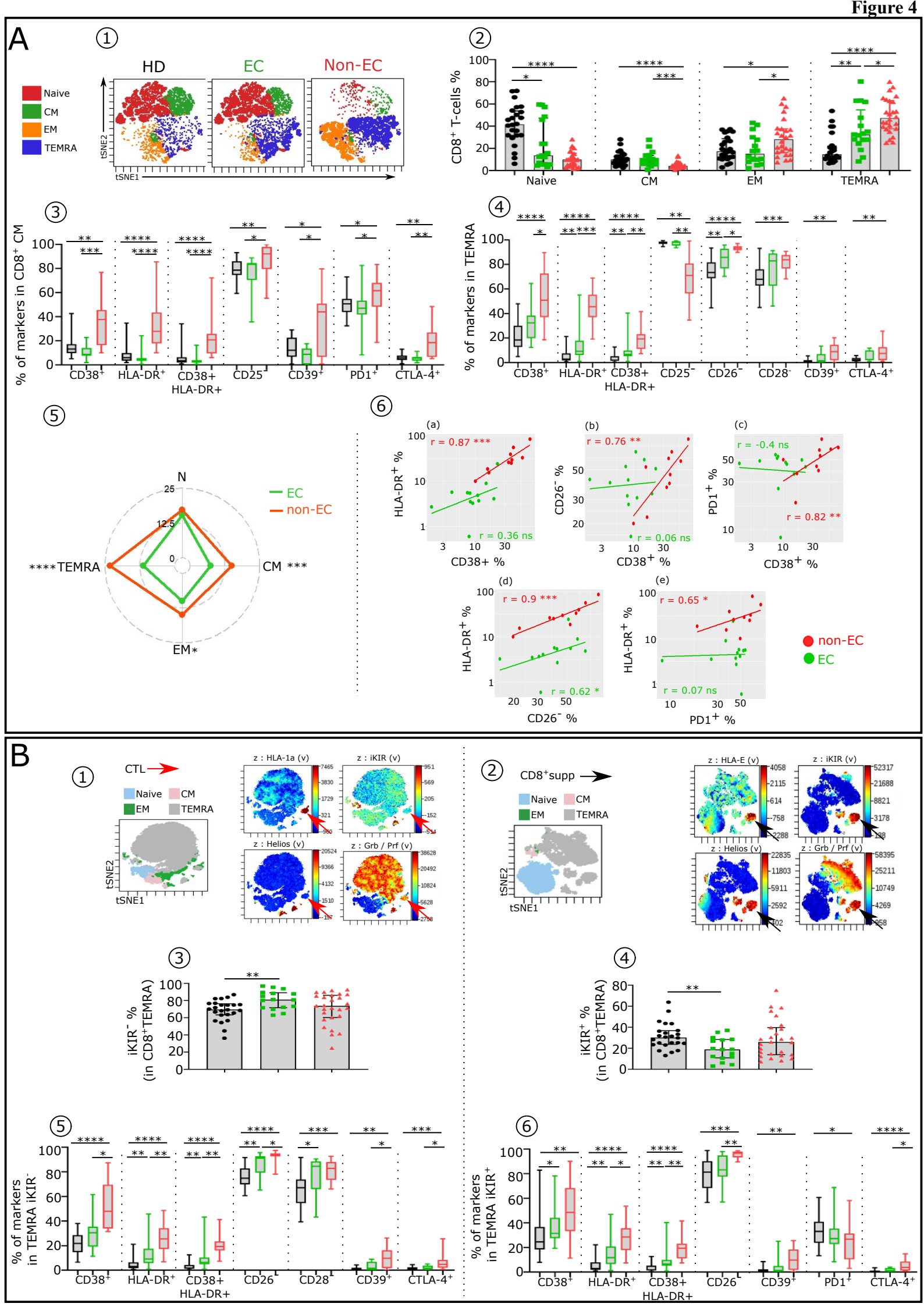
A
1
HD
EC
Non-EC
Naive
CM
EM
TEMRA
tSNE2
tSNE1
2
CD8+ T-cells %
Naive
CM
EM
TEMRA
3
% of markers in CD8+ CM
CD38+
HLA-DR+
CD38+ HLA-DR+
CD25-
CD39+
PD1+
CTLA-4+
4
% of markers in TEMRA
CD38+
HLA-DR+
CD38+ HLA-DR+
CD25-
CD26-
CD28-
CD39+
CTLA-4+
5
N
EC
non-EC
****TEMRA
CM ***
EM*
6
(a)
r = 0.87 ***
r = 0.36 ns
HLA-DR+ %
CD38+ %
(b)
r = 0.76 **
r = 0.06 ns
CD26- %
CD38+ %
(c)
r = -0.4 ns
r = 0.82 **
PD1+ %
CD38+ %
(d)
r = 0.9 ***
r = 0.62 *
HLA-DR+ %
CD26- %
(e)
r = 0.65 *
r = 0.07 ns
HLA-DR+ %
PD1+ %
non-EC
EC
B
1
CTL
Naive
CM
EM
TEMRA
tSNE2
tSNE1
z : HLA-1a (v)
z : iKIR (v)
z : Helios (v)
z : Grb / Prf (v)
2
CD8+supp
Naive
CM
EM
TEMRA
tSNE2
tSNE1
z : HLA-E (v)
z : iKIR (v)
z : Helios (v)
z : Grb / Prf (v)
3
iKIR- % (in CD8+TEMRA)
4
iKIR+ % (in CD8+TEMRA)
5
% of markers in TEMRA iKIR-
CD38+
HLA-DR+
CD38+ HLA-DR+
CD26-
CD28-
CD39+
CTLA-4+
6
% of markers in TEMRA iKIR+
CD38+
HLA-DR+
CD38+ HLA-DR+
CD26-
CD39+
PD1+
CTLA-4+

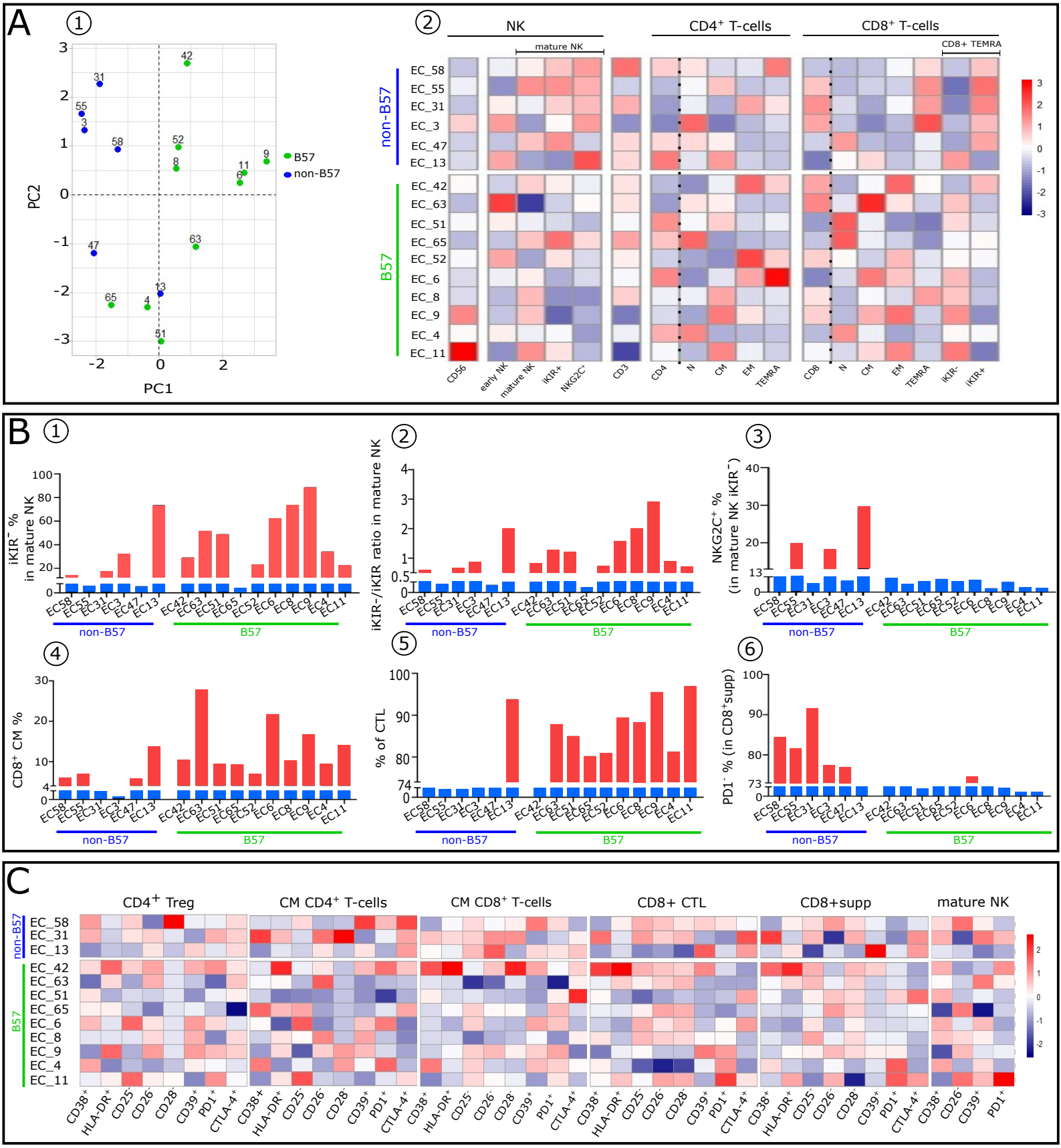
A
PC1
PC2
B57
non-B57
NK
CD4+ T-cells
CD8+ T-cells
mature NK
CD8+ TEMRA
non-B57
B57
CD56
early NK
mature NK
iKIR+
NKG2C+
CD3
CD4
N
CM
EM
TEMRA
CD8
iKIR-
iKIR+
B
iKIR- % in mature NK
iKIR-/iKIR ratio in mature NK
NKG2C+ % (in mature NK iKIR-)
CD8+ CM %
% of CTL
PD1- % (in CD8+supp)
C
CD4+ Treg
CM CD4+ T-cells
CM CD8+ T-cells
CD8+ CTL
CD8+supp
mature NK

Figure 5

Extended data Tables and Figures:

Extended data Table 1: IFN type I effects on immune cell subtypes and its correlation with suppressive cytokines.

A-Known potential pathologic effects during chronic viral infection of IFN type I

Cellular mechanism	Cell type	effects	References
Homeostasis	T-cells	Inhibits IL-7 signaling pathway	*(39,7)*
Proliferation	T-cells	Inhibits T-cell proliferation	*(40)*
Hyper-activation	T-cells	Increases of CD38, HLA-DR	*(41,42,27,43)*
Loss of function	T-cells	Enhances PD-1 expression	*(44,43,45,46)*
		Decreases CD25 expression	*(47)*
		Decreases CD28 expression	*(48)*
	DCs and other APCs	Upregulates PD-L1, IL-10	*(49,50)*
Apoptosis	T-cells	Enhances expression of CD95, Bak, TRAIL	*(51,52,53)*
	DCs and other APCs	Upregulates and pro-apoptotic molecules	*(54,55)*
Involution		Induces thymic involution	*(35,56)*

B-Known correlation between IFN type I and immune suppressive cytokines

Suppressive cytokine	effects	References
TGF-β1	IFNα enhances TGF-β1 signaling pathways	*(57)*
IL-10	IFNα promotes $CD4^+$T-cells differentiation into suppressive IL-10 secreting Tr1 cells	*(9,10)*

Extended data Table 2: Clinical data for HIV patients

Table 2a : EC patients

EC	HIV dx	Sample date	CD4 at sample date	VL	HLA B57	Sex	Race	HIV risk factor
3	1991	10/12/012	1140	334	-	M	AA	IDU
4	1993	22/08/2011	952	<40	+	F	AA	HS
6	1992	31/05/2011	1889	<75	+	F	AA	IDU
8	1989	01/02/2010	1018	<40	+	M	AA	IDU
9	2003	25/09/2014	496	<40	+	M	AA	IDU
11	1997	10/72/011	917	<40	+	M	AA	IDU
13	1993	21/02/2012	864	<40	-	M	AA	IDU
31	1992	23/05/2012	587	<48	-	M	AA	MSM
32	2000	23/05/2012	643	<48	-	F	AA	IDU
42	1990	13/11/2013	731	<220	+	M	AA	IDU
47	2007	01/12/2013	891	<20	-	F	AA	IDU
51	2007	20/10/2014	1250	<40	+	F	AA	HS
52	1992	01/08/2012	340	<20	+	M	AA	IDU
55	1994	01/02/2013	482	50	-	M	AA	IDU
58	1991	01/03/2013	1745	59	-	F	AA	HS
63	1988	24/01/2014	632	32	+	F	AA	IDU
65	1991	01/06/2013	1792	<48	+	M	AA	HS
68	2002	01/07/2010	584	169	+	F	AA	HS

Table 2b : non-EC patients

Untreated patients study_ID	sample date	CD4 at sample date	VL	Origin
1	03/11/2004	506	23808	NIH (Bethesda)
2	22/04/2004	516	58059	
3	01/10/2005	230	153719	
4	27/09/2005	327	132773	
5	19/06/2006	419	1715	
6	04/10/2007	513	12015	
7	13/08/2007	447	21701	
8	13/03/2008	319	4785	
9	05/11/2011	756	7011	
SS_20	08/10/2005	445	407	
SS_21	11/10/2009	292	3012	
SS_22	10/07/2010	477	29257	
SS_23	07/22/08	639	<50	
SS_24	11/17/2008	267	26059	
SS_25	03/23/2006	470	5384	
SS_26	11/07/2012	740	11417	
SS_27	01/28/2014	344	63954	
SS_28	11/04/2010	872	7180	
SS_29	12/03/2002	196	17809	
AZT70934	12/03/2021	470	2480	Laboratoire de Référence SIDA (Liège)
AZT71312=1373	12/03/2021	100	24800	
AZT_71320_AFCHM_6	12/08/2020	139	32800	
AZT_71333_KWGIF_7	12/09/2021	356	9790	
AZT_71374_DIAMM_8		390	588000	
AZT_71391_GAFUM_9	02/24/2021	1064	14700	
AZT71422	03/05/2021	30	850000	
AZT_72336_GEMAM_11		20	824	
AZT_72498_YOLEF_12		280	82700	
AZT_72607_CHUIN	03/16/2021	577	157000	
AZT_72644_NGNNF	03/18/2021	180	73700	

Extended data Table 3: mAb list

Table 3a: mAb lis for the immune cells culture phenotype

Markers	Fluorochrome	Clone	Origin
CD3	AF532	UCHT1	Invitrogen
CD4	BV510	RPA-T4	BioLegend
CD8	BV750	RPA-T8	BioLegend
CD25	BV786	M-A251	BD Biosciences
CD38	PerCPeF710	HB7	Invitrogen
CD56	BV711	HCD56	BioLegend
CD16	Ef450	eBioCB163	Invitrogen
NKG2D	PE	AD11	BD Biosciences
CD95	BV421	DX2	BD Biosciences
7AAD	7AAD		Sigma Aldrich

Table 3b: mAb lis for the immune cells panel

	Markers	Fluorochrome	Clone	Origin
Immune cell types	CD3	AF532	UCHT1	Invitrogen
	CD4	BV510	RPA-T4	BioLegend
	CD8	BV750	RPA-T8	BioLegend
	CD56	BV711	HCD56	BioLegend
	CD16	Ef450	eBioCB163	Invitrogen
	TCR-γδ	BV480	11F2	BD Biosciences
	CD19	BV750	HIB19	Biolegend
	CD14	AF647	MOP9	BD Biosciences
	CD123	PerCpCy5.5	7G3	BD Pharmingen
	CD11c	BV605	3.9	BioLegend
Immune Activation / Maturation	CD45RA	FITC	REA562	Miltenyi Biotech
	CCR7	BV421	G043H7	Biolegend
	CD28	APC-R700	CD28.2	BD Biosciences
	CD25	BV786	M-A251	BD Biosciences
	HLA-DR	APCCy7	1243	Biolegend
	CD26	PE	BA5b	Biolegend
	CD39	PeCy7	A1	BioLegend
	CD38	PerCPeF710	HB7	Invitrogen
Immune checkpoint	PD1	BV650	EH12.2H7	BioLegend
	CTLA-4	PeCy5	BNI3	BD Biosciences
	KIR2DL1	APC	REA284	Miltenyi Biotech
	KIR3DL1/DL2	APC	REA970	Miltenyi Biotech
	KIR2DL2/DL3	APC	DX27	Miltenyi Biotech
	KIR2DL5	APC	REA955	Miltenyi Biotech
T-cell function	Foxp3	PeCF	236A/E7	BD Biosciences
Viability	Zombie	NIR		Biolegend

Table 3c: mAb lis for CD8⁺ T-cells panel

	Markers	Fluorochrome	Clone	Origin
Immune cell types	CD3	AF532	UCHT1	Invitrogen
	CD4	BV510	RPA-T4	BioLegend
	CD8	BV570	RPA-T8	BioLegend
	CD56	APC-Cy7	HCD56	BioLegend
Immune Activation / Maturation	CD45RA	BV421	HI100	BioLegend
	CCR7	BV785	G043H7	BioLegend
	CD28	APC-R700	CD28 .2	BD Biosciences
	Hélios	PE-Dazzle594	22F6	BioLegend
Immune checkpoint	NKG2A	PE-Vio770	REA110	Miltenyi Biotech
	KIR2DL1	APC	REA284	Miltenyi Biotech
	KIR3DL1/DL2	APC	REA970	Miltenyi Biotech
	KIR2DL2/DL3	APC	DX27	Miltenyi Biotech
	KIR2DL4	APC	REA768	Miltenyi Biotech
	KIR2DL5	APC	REA955	Miltenyi Biotech
	NKG2C	VioBright	REA205	Miltenyi Biotech
	Nkp30	PE-Cy5	Z25	Beckman Coulter
	Nkp44	PE-Cy5	Z231	Beckman Coulter
	Nkp46	PE-Cy5	BAB281	Beckman Coulter
	PD1	BV650	EH12.2H7	BioLegend
Viability	zombie	NIR		BioLegend

Table 3d: mAb lis for cytotoxic CD8⁺ T-cells panel

	Markers	Fluorochrome	Clone	Origin
Immune cell types	CD45	PerCP	HI30	BioLegend
	CD3	AF532	UCHT1	Invitrogen
	CD4	BV510	RPA-T4	BioLegend
	CD8	BV570	RPA-T8	BioLegend
	CD56	APC-Cy7	HCD56	BioLegend
CD8+ cytotoxic T-cells	HLA1-a	BV711	pentamer	Proimmune
	HLA-E	PE	E*01 :01	Proimmune
Immune Activation / Maturation	CD45RA	BV421	HI100	BioLegend
	CCR7	BV785	G043H7	BioLegend
	CD28	APC-R700	CD28 .2	BD Biosciences
	Helios	PE-Dazzle594	22F6	BioLegend
	Nkp30	PE-Cy5	Z25	Beckman Coulter
	Nkp44	PE-Cy5	Z231	Beckman Coulter
	Nkp46	PE-Cy5	BAB281	Beckman Coulter
Immune checkpoint	NKG2A	PE-Vio770	REA110	Miltenyi Biotech
	KIR2DL1	APC	REA284	Miltenyi Biotech
	KIR3DL1/DL2	APC	REA970	Miltenyi Biotech
	KIR2DL2/DL3	APC	DX27	Miltenyi Biotech
	KIR2DL5	APC	REA955	Miltenyi Biotech
	NKG2C	VioBright	REA205	Miltenyi Biotech
	PD1	BV650	EH12.2H7	BioLegend
Imune cell function	GrzB/perf	PerCP-cy5.5	QA16A02/B-D48	Biolegend
Viability	zombie	NIR		BioLegend

Extended data Figure Legends

Extended data Fig. 1: Effect of IFNα and IFNλ2 on stimulated CD4$^+$T-cells from HD.

CD4$^+$T-cells (1.5×10^5 per well) were stimulated with platebound anti-CD3 mAb (pbαCD3) (4 μg/mL) in presence of soluble anti-CD28 mAb (sαCD28) (4 μg/mL) and IL-2 (100 IU/mL) for 4 days. (**A1**) Representative FACS histograms displaying IFNα effect on CD4$^+$T-cell proliferation measured by CFD dilution assay. (**A2**) Histograms showing dose–effect of IFNα and IFNλ2 on the frequency of CFD^{low} cells (n=4). (**A1**) Representative FACS histograms displaying IFNα effect on apoptosis of 4 d-stimulated CD4$^+$T-cells evaluated by 7-amino-actinomycin D (7-AAD) staining. (**B2**) Histograms showing dose–effect of IFNα and IFNλ2 on the frequency of 7-AAD$^+$ cells (n=4). (**C1**) Representative FACS histograms displaying IFNα effect on CD38 expression on 4 d-stimulated CD4$^+$T-cells. Histograms showing the IFNα and IFNλ2 dose–effect on (**C2**) the CD38 frequency and (**C3**) the CD38 Mean Fluorescence Intensity (MFI) in CD4$^+$ T cells (n=4). (**C4**) Representative FACS histograms displaying IFNα effect on CD25 expression on 4 d-stimulated CD4$^+$T-cells. Histograms showing the IFNα and IFNλ2 dose–effect on (**C5**) the CD25 frequency and (**C6**) the CD25 MFI in CD4$^+$T-cells (n=4).

Extended data Fig. 2: Effect of IFNα and IFNλ2 on the IL-10 secretion by stimulated CD4$^+$T-cells from HD.

CD4$^+$T-cells (1.5×10^5 per well) were stimulated with pbαCD3 (4 μg/mL) in presence of soluble sαCD28 (4 μg/mL) and IL-2 (100 IU/mL) for 4 days. IL-10 levels were quantified by Luminex technology in the 4-d culture supernatant of stimulated CD4$^+$T-cells (n=3).

Extended data Fig. 3: Gating strategy for immune cell types and specific markers analysed in each immune cell subsets.

A- Gating strategy for immune cell types. The gating strategy used to identify the main cellular subsets is presented. Arrows are used to visualize the relationships across plots, and numbers are used to call attention to populations described here. After doublets and dead cells were excluded, lymphocytes were gated based on FSC-A/SSC-A properties. From the $CD14^{-}CD19^{-}$ lymphocyte gate, the following populations were identified: $CD3^{+}TCR\gamma\delta^{+}$, $TCR\gamma\delta^{-}$ were subdivided in $CD3^{-}$ and $CD3^{+}$T-cells. NK-cells were defined as $CD3{-}TCR\gamma\delta{-}HLA\text{-}DR{-}$ and classified as early NK ($CD56^{+}CD16{-}$), mature NK ($CD56^{+}CD16^{+}$), and terminal NK ($CD56{-}CD16^{+}$) cells. The $CD3^{+}TCR\gamma\delta{-}$ population was divided in $CD4^{+}$ and $CD8^{+}$ T-cells. In $CD4^{+}$T-cells subpopulation, $CCR7^{+}$ and $CD45RA^{+}$ were used to further classify these cells in four subpopulations: N ($CCR7^{+}CD45RA^{+}$), CM ($CCR7^{+}CD45RA^{-}$), EM ($CCR7^{-}CD45RA^{-}$) and TEMRA ($CCR7^{-}CD45RA^{+}$). Tregs were identified from the $CD4^{+}$ population using Foxp3 expression. $Foxp3^{+}$ cells were classified in naïve and memory Treg cells using CD45RA and CD25 markers. $CD45RA^{-}CD25^{+}$ represent the memory Treg cells population. As for $CD4^{+}$T-cells, $CD8^{+}$T-cells were classified using CD45RA and CCR7 markers: four populations were identified: N ($CCR7^{+}CD45RA^{+}$), CM ($CCR7^{+}CD45RA^{-}$), EM ($CCR7^{-}CD45RA^{-}$) and TEMRA ($CCR7^{-}CD45RA^{+}$). Among TEMRA $CD8^{+}$T-cells, we distinguished two cytotoxic subpopulations: $iKIR^{+}$ ($CD8^{+}$supp) and $iKIR^{-}$ (CTL). Dendritic cells (DCs) were identified by gating on $CD3^{-}CD19^{-}CD56^{-}CD14^{-}HLA\text{-}DR^{+}$ and from there $CD123^{+}CD11c^{-}$ (pDCs) and $CD11c^{+}CD123^{-}$ mDCs were identified.

B- Specific markers analysed in each immune cell subsets.

Extended data Fig. 4: Immune cell types of non-EC but not of EC involved in the innate phase of an anti-HIV IR exhibit distinct altered pattern linked to elevated IFNα.

(A) Representative dot plot showing how to distinguish pDC ($CD123^+CD11c^-$) and mDC ($CD123^-CD11C^+$) subsets within the HLA-DR^+lin^- population in HD **(A1).** Histograms showing the frequencies of pDC **(A2)** and the pDC:mDC ratio **(A3)** across the groups (HD n=22, EC n=12 and non-EC n=8). (**B**) Specific markers proportion on TCR γδ T-cells of each studied group (HD n=22, EC n=12 and non-EC n=8)**.** (**C**) Histograms showing the frequencies of CCR7 in $CD4^+$ (C1) and $CD8^+$ (C2) T-cells across the groups (HD n=22, EC n=12 and non-EC n=26). Scatterplots showing relationships between the frequencies of $CD4^+$CM (C3) and $CD8^+$CM (C4) T-cells with IFNα levels in HIV-1-infected patients. (C5) Histograms showing the frequencies of $CD8^+$CM in HD (n=22), HLA-$B57^+$ EC (n=10), HLA-$B57^-$ EC (n=6) and non-EC (n=26). Significance was determined by unpaired Mann-Whitney U test. *P<0.05, **P<0.01, ***P<0.001, ****P<0.0001.

Extended data Fig. 5: Frequency and phenotypic alterations of $CD4^+$T-cell subsets in non-EC and EC

Boxplots showing the expression of indicated marker in $CD4^+$Naïve (**a**), EM (**b**) and TEMRA (**c**) across the groups (HD n=22, EC n=12 and non-EC n=8). (**d**) Radar chart showing a composite score of phenotypic cell alteration calculated for each $CD4^+$Tconv subpopulation in non-EC and EC (see Methods). (**e**) Scatterplots showing relationships between the expression level of indicated markers in the $CD4^+$CM subsets (EC n=12 and non-EC n=8). Correlations were evaluated with Spearman's rank correlation test. Significance was determined by unpaired Mann-Whitney U test. *P<0.05, **P<0.01, ***P<0.001, ****P<0.0001.

Extended data Fig. 6: Frequency of CTL and CD8$^+$supp in EC-B57$^+$, EC-B57$^-$, non-EC and HD.

Histograms showing distributions of CTL and CD8$^+$supp between HD (Black, n=24), EC-B57$^+$ (green, n=10), EC-B57$^-$ (purple and blue, n=6) and non-EC (red, n=26). One EC-B57$^-$ (EC13) in blue behaves as an EC-B57$^+$. Significance was determined by unpaired Mann-Whitney U test. *P<0.05, **P<0.01, ***P<0.001, ****P<0.0001.

Extended data Fig. 7: NK-cell cytotoxic activity varies in HIV-infected patients according to their status.

1-Left: in non-EC, NK-cells are inactive given the high frequency of their inhibitory checkpoints leading to a state of exhaustion in large part induced by IFNα.

2- Right and up: in HLA-B57$^+$ EC NK-cells, which possess negligible iKIR and further express negligible inhibitory receptors, lyse infected target cells expressing HLA-B restricted HIV-peptides.

3-Right and down: in HLA-B57$^-$ EC NK-cells, which express iKIR, but have negligible inhibitory checkpoints, express the activating NKG2C receptor, counterbalancing the iKIR signaling, and can thereby kill infected cells carrying HIV-peptides in an HLA-E restriction.

Figure created with Biorender.

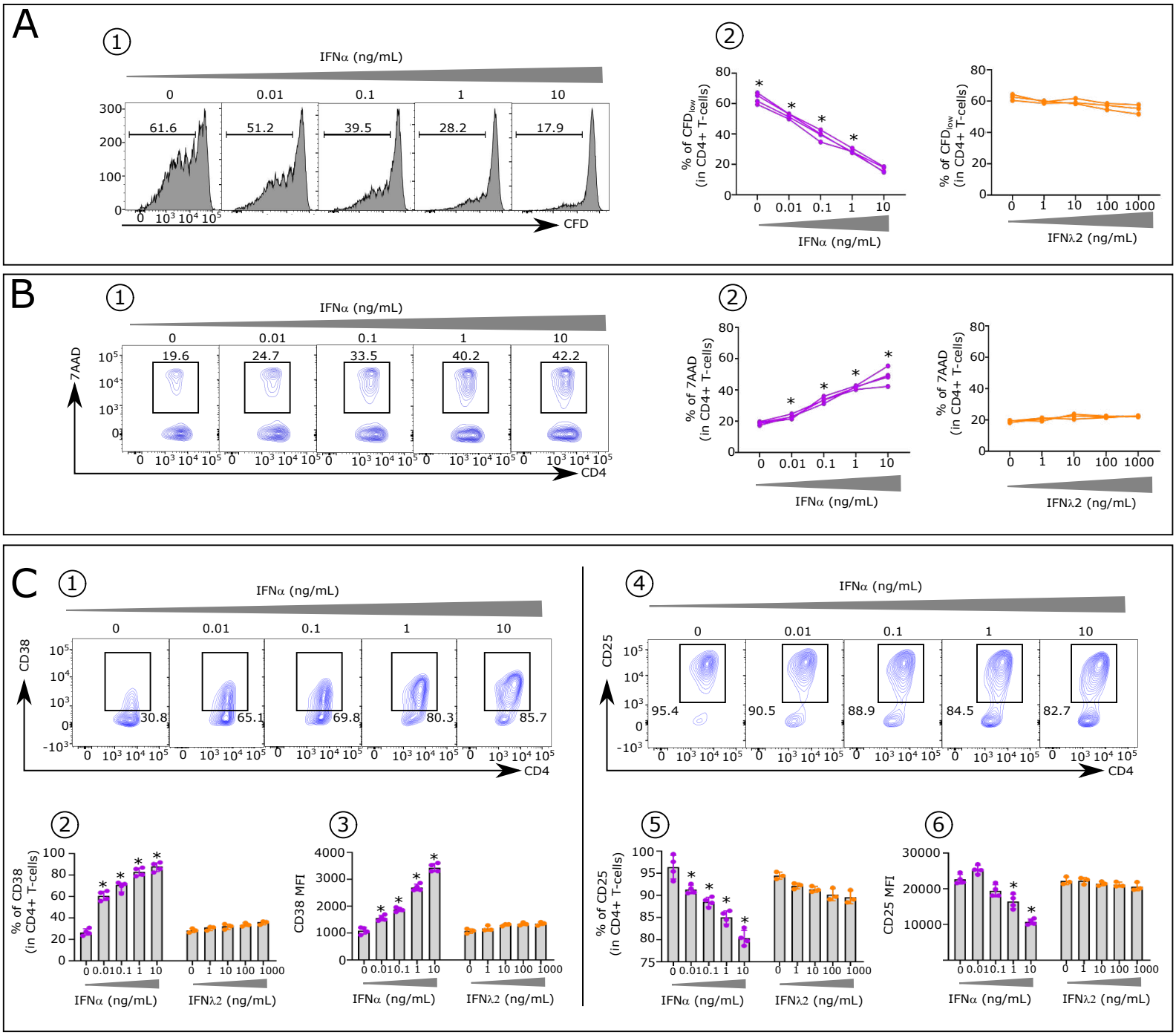

Extended data Fig. 1

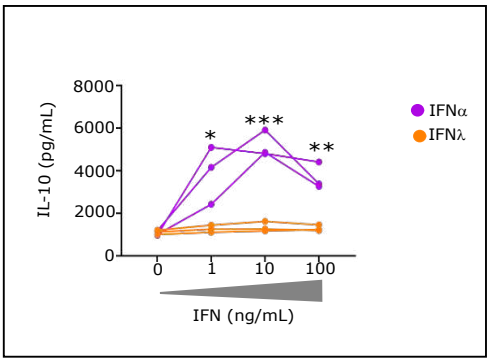

Extended data Fig. 2

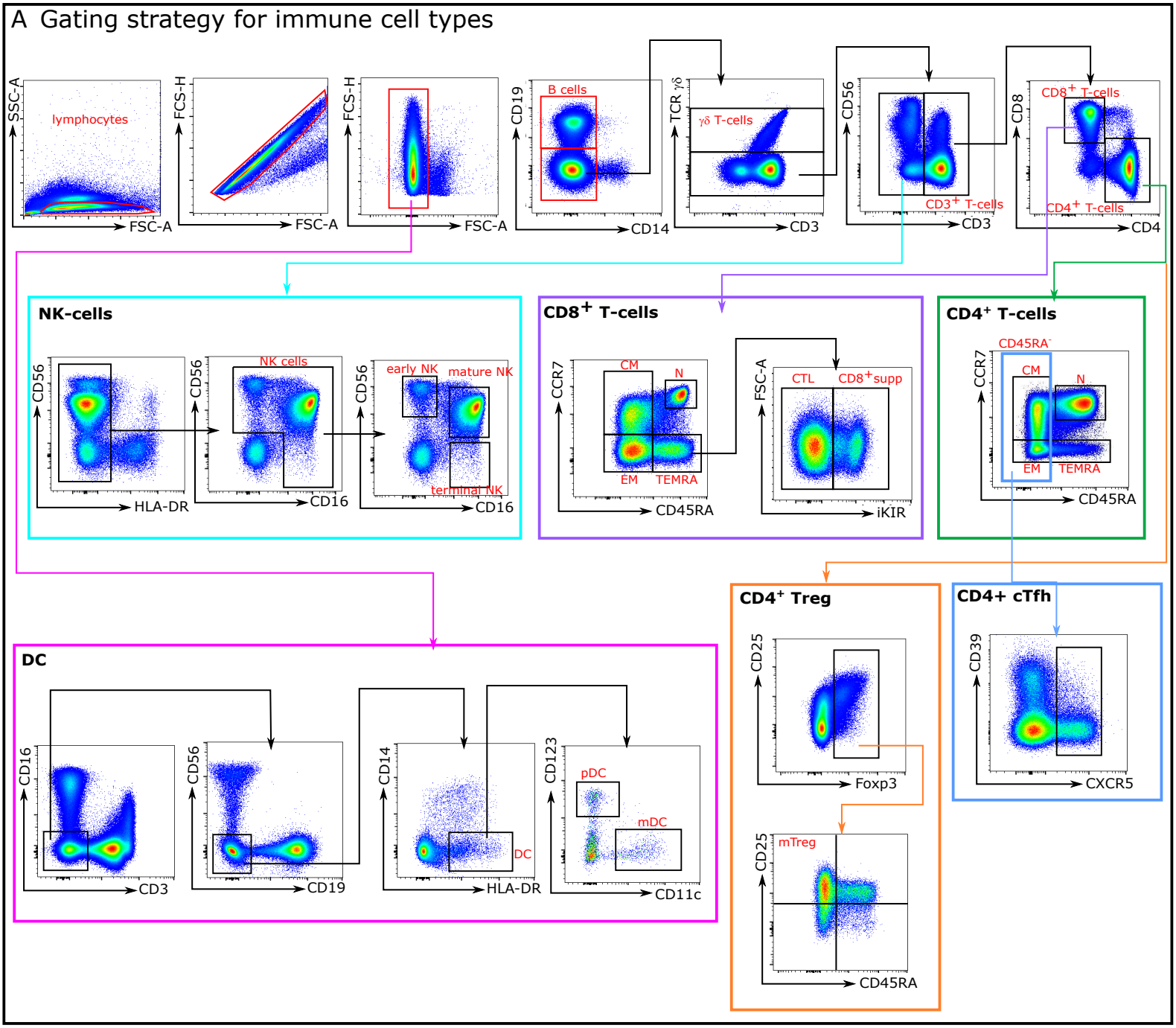

B Specific markers analysed in each immune cell subsets

Immune activation / Maturation
CD25, CD28, HLA-DR,
CD26, CD39, CD38, CD95 and Helios

Immune checkpoint
PD1, CTLA-4, iKIR, NKG2A,
NKG2C, NCR, NKG2D

Immune cell function
GrzB/perf, Foxp3

Extended data Fig. 3

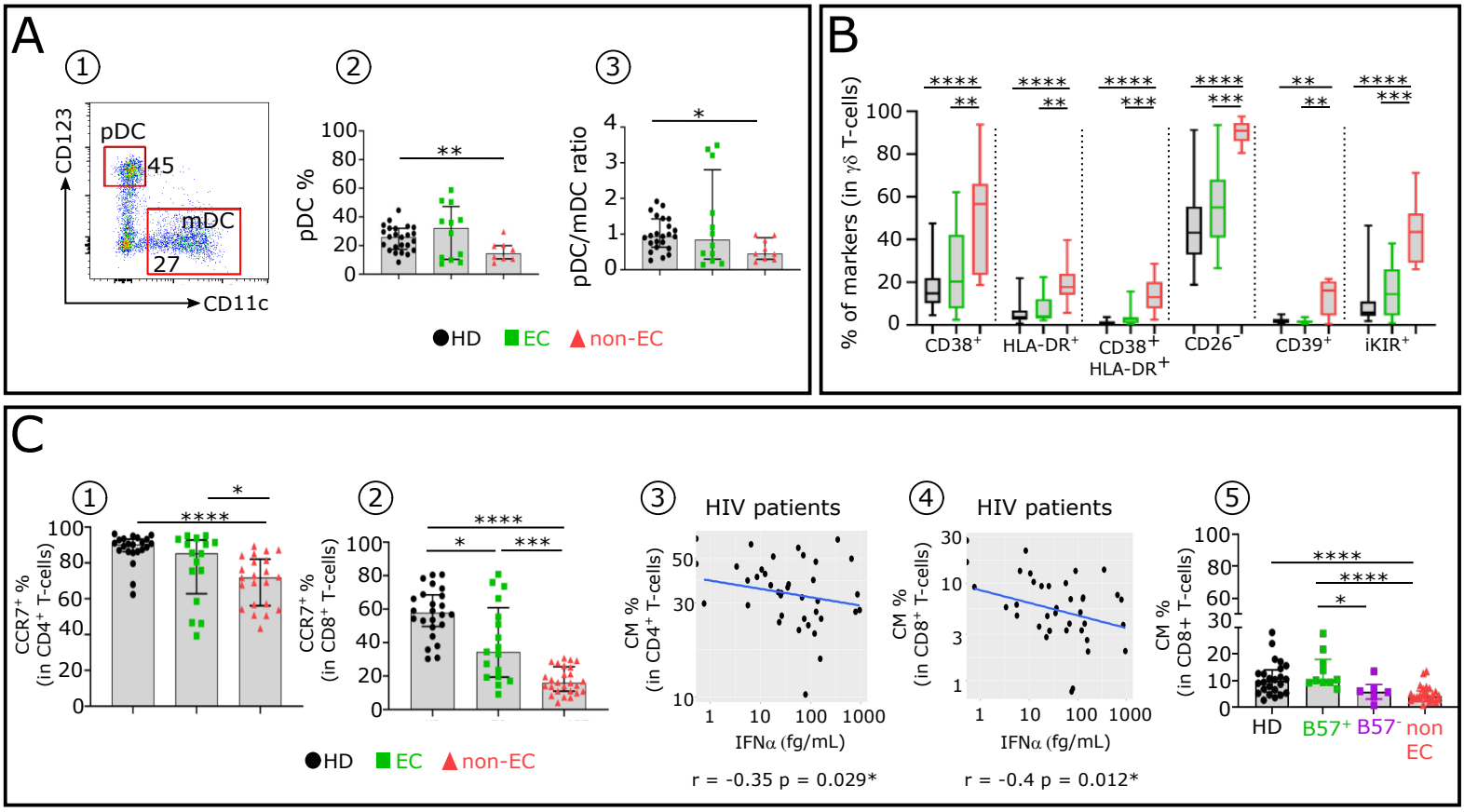

Extended data Fig. 4

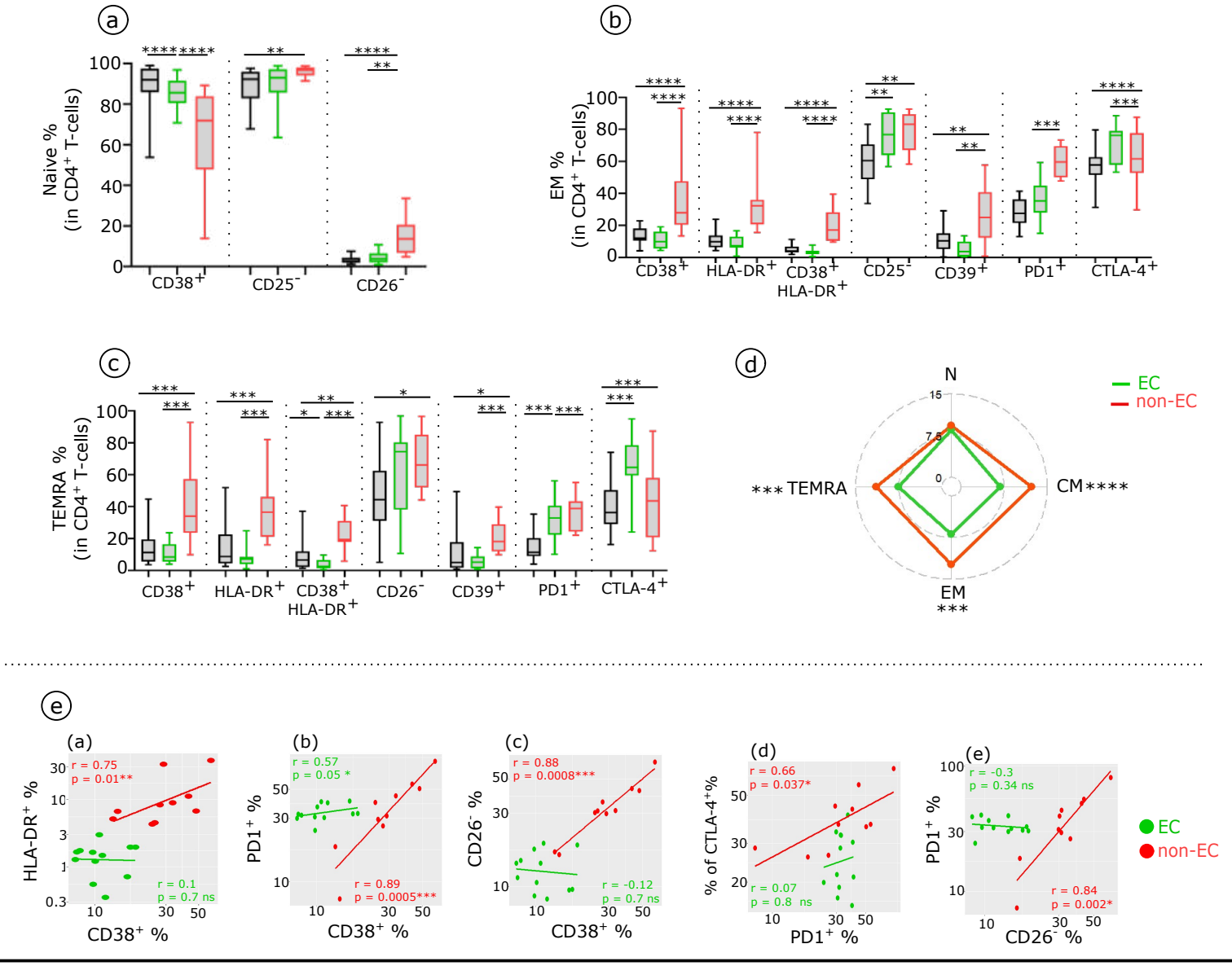

Extended data Fig. 5

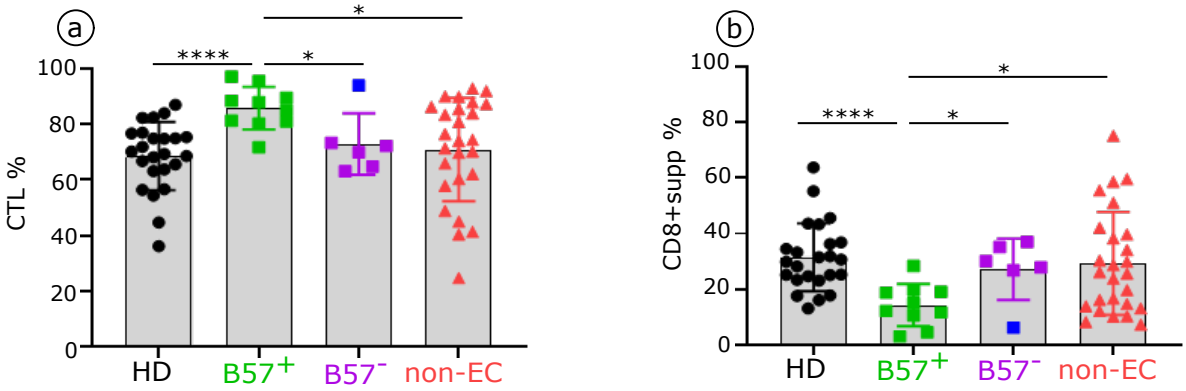

Extended data Fig. 6

Extended data Fig. 7